

Accurate fundamental parameters for 23 bright solar-type stars

H. Bruntt^{1,2*}, T. R. Bedding², P.-O. Quirion^{3,4}, G. Lo Curto⁵, F. Carrier⁶, B. Smalley⁷,
T. H. Dall⁸, T. Arentoft⁴, M. Bazot⁹, R. P. Butler¹⁰

¹LESIA, Observatoire de Paris-Meudon, 92195, France

²Sydney Institute for Astronomy, School of Physics, The University of Sydney, 2006 NSW, Australia

³Canadian Space Agency, 6767 Boulevard de l'Aéroport, Saint-Hubert, Québec J3Y 8Y9, Canada

⁴Danish AsteroSeismology Centre (DASC), Department of Physics and Astronomy, University of Aarhus, DK-8000 Aarhus C, Denmark

⁵European Southern Observatory, Alonso de Cordova 3107, Vitacura, Santiago, Chile

⁶Instituut voor Sterrenkunde, Katholieke Universiteit Leuven, Belgium

⁷Astrophysics Group, Keele University, Keele, Staffordshire ST5 5BG, UK

⁸European Southern Observatory, Karl Schwarzschild Str. 2, 85748 Garching bei München, Germany

⁹Universidade do Porto, Centro de Astrofísica, Rua das Estrelas, PT 4150-762 Porto, Portugal

¹⁰Carnegie Institution of Washington, Department of Terrestrial Magnetism, 5241 Broad Branch Road NW, Washington, DC 20015-1305, USA

Accepted XXX February 2010. Received ZZZZ December 2009

ABSTRACT

We combine results from interferometry, asteroseismology and spectroscopy to determine accurate fundamental parameters of 23 bright solar-type stars, from spectral type F5 to K2 and luminosity classes III to V. For some stars we can use direct techniques to determine the mass, radius, luminosity and effective temperature, and we compare with indirect methods that rely on photometric calibrations or spectroscopic analyses. We use the asteroseismic information available in the literature to infer an indirect mass with an accuracy of 4–15%. From indirect methods we determine luminosity and radius to 3%. We find evidence that the luminosity from the indirect method is slightly overestimated ($\approx 5\%$) for the coolest stars, indicating that their bolometric corrections are too negative. For T_{eff} we find a slight offset of -40 ± 20 K between the spectroscopic method and the direct method, meaning the spectroscopic temperatures are too high. From the spectroscopic analysis we determine the detailed chemical composition for 13 elements, including Li, C and O. The metallicity ranges from $[\text{Fe}/\text{H}] = -1.7$ to $+0.4$, and there is clear evidence for α -element enhancement in the metal-poor stars. We find no significant offset between the spectroscopic surface gravity and the value from combining asteroseismology with radius estimates. From the spectroscopy we also determine $v \sin i$ and we present a new calibration of macro- and microturbulence. From the comparison between the results from the direct and spectroscopic methods we claim that we can determine T_{eff} , $\log g$, and $[\text{Fe}/\text{H}]$ with absolute accuracies of 80 K, 0.08 dex, and 0.07 dex. Photometric calibrations of Strömgen indices provide accurate results for T_{eff} and $[\text{Fe}/\text{H}]$ but will be more uncertain for distant stars when interstellar reddening becomes important. The indirect methods are important to obtain reliable estimates of the fundamental parameters of relatively faint stars when interferometry cannot be used. Our study is the first to compare direct and indirect methods for a large sample of stars, and we conclude that indirect methods are valid, although slight corrections may be needed.

Key words: stars: fundamental parameters stars: late type – stars: abundances.

1 INTRODUCTION

Rapid progress in the fields of exoplanet science and asteroseismology has given renewed importance to the task of determining fundamental stellar parameters. The two main parameters that describe the evolution and structure of a star are mass and chemical composition. Additional stellar parameters include the radius, luminosity,

and rotation rate, all of which change during the evolution of the star. The composition of a star will also change during its evolution due to fusion in the core, mixing from rotation, overshooting and diffusion. In later evolutionary stages, the effects of deep convection dredge-up and mass loss become important. The fundamental parameters of stars can be determined using various techniques like stellar interferometry (to obtain the radius and effective temperature) and radial velocities and light curves of detached eclipsing binary stars (to get mass and radius). These methods are important

* E-mail:bruntt@phys.au.dk

Table 1. Observable properties of the target stars. V is from SIMBAD and parallaxes are all from van Leeuwen (2007) except α Cen A+B which is from Söderhjelm (1999). The f_{bol} is determined in Sect. 3.2. The BC is from VandenBerg & Clem (2003) and have an uncertainty of 0.03 mag. For four stars $\Delta\nu$ has not been measured and we give approximate values found using Eq. 2 (indicated by the \approx symbol). References for the angular diameters and the asteroseismic data are given in the last two columns and explained in detail below the Table.

Star	HD	V	π_{p} [mas]	θ_{LD} [mas]	f_{bol} [nW m $^{-2}$]	BC	ν_{max} [mHz]	$\Delta\nu$ [μ Hz]	Ref. θ_{LD}	Ref. Seis.
β Hyi	2151	2.80	134.07 ± 0.11	2.257 ± 0.019	1.970 ± 0.073	-0.07	1.00	57.5	1	i
τ Cet	10700	3.49	273.96 ± 0.17	2.022 ± 0.011	1.140 ± 0.038	-0.18	4.50	169.0	2	l
ι Hor	17051	5.41	58.24 ± 0.22			-0.02	2.70	120.0		m
α For	20010	3.85	70.24 ± 0.45			-0.05	1.10	≈ 57		i
δ Eri	23249	3.51	110.62 ± 0.22	2.394 ± 0.029	1.180 ± 0.046	-0.26	0.70	43.8	3	b
α Men	43834	5.09	98.05 ± 0.14			-0.10				
Procyon A	61421	0.34	284.52 ± 1.27	5.446 ± 0.031	17.600 ± 0.483	+0.00	1.00	55.0	4	j
171 Pup	63077	5.37	65.75 ± 0.51			-0.12	2.05	97.1		d
ξ Hya	100407	3.55	25.14 ± 0.16	2.386 ± 0.021	1.170 ± 0.046	-0.24	0.09	6.8	3	g
β Vir	102870	3.63	91.50 ± 0.22	1.450 ± 0.018	0.915 ± 0.032	-0.02	1.40	72.1	5	e
η Boo	121370	2.70	87.77 ± 1.24	2.204 ± 0.011	2.140 ± 0.063	-0.01	0.75	39.9	6	h
α Cen A	128620	0.00	747.10 ± 1.20	8.511 ± 0.020	26.300 ± 0.900	-0.06	2.40	106.2	7	i
α Cen B	128621	1.33	747.10 ± 1.20	6.001 ± 0.034	8.370 ± 0.349	-0.22	4.10	161.4	7	i
HR 5803	139211	5.95	32.32 ± 0.50			-0.02	1.80	85.0		d
γ Ser	142860	3.85	88.85 ± 0.18			-0.04	1.60	≈ 79		i
μ Ara	160691	5.15	64.48 ± 0.31			-0.08	2.00	90.0		c
70 Oph A	165341	4.03	196.66 ± 0.84			-0.17	4.50	161.7		f
η Ser	168723	3.26	53.93 ± 0.18			-0.33	0.13	8.0		a
β Aql	188512	3.70	73.00 ± 0.20	2.180 ± 0.090	0.979 ± 0.032	-0.25	0.41	≈ 26	8	i
δ Pav	190248	3.56	163.71 ± 0.17			-0.10	2.30	≈ 106		i
γ Pav	203608	4.22	107.98 ± 0.19			-0.09	2.60	120.4		k
τ PsA	210302	4.95	54.70 ± 0.28			-0.01	1.95	89.5		d
ν Ind	211998	5.29	34.84 ± 0.27			-0.25	0.32	25.1		i

References for θ_{LD} :

1=North et al. (2007); 2=Teixeira et al. (2009); 3=Thévenin et al. (2005); 4=Kervella et al. (2004), Mozurkewich et al. (2003), and Nordgren et al. (2001); 5=North et al. (2009); 6=Thévenin et al. (2005), Mozurkewich et al. (2003), Nordgren et al. (2001), and van Belle et al. (2007); 7=Kervella et al. (2003); 8=Nordgren et al. (1999).

References for ν_{max} and $\Delta\nu$:

a=Barban et al. (2004); b=Bouchy & Carrier (2003); c=Bouchy et al. (2005); d=F. Carrier (private communication); e=Carrier et al. (2005), f=Carrier & Eggenberger (2006); g=Frandsen et al. (2002); h=Carrier et al. (2005); i=Kjeldsen et al. (2008); j=Arentoft et al. (2008); k=Mosser et al. (2008); l=Teixeira et al. (2009); m=Vaclair et al. (2008).

2.1 Mass from a binary orbit

The absolute masses of stars in binary systems are determined from astrometric or radial velocity measurements by applying Kepler's laws. This is possible for four of the stars in our sample: Procyon A (Girard et al. 2000; Gatewood & Han 2006), α Cen A and B (Pourbaix et al. 2002), and 70 Oph A (Eggenberger et al. 2008). In Table 2 we list the measured masses (column 2). In the case of Procyon A we give the weighted mean of the two studies mentioned above. These four stars provide an important test for the indirect method for mass determination that we propose in the following.

2.2 Mass from asteroseismic data

The mass of a solar-type star can be inferred using asteroseismology (e.g. North et al. 2007). The power spectrum of the observed time-series of radial velocities or a photometric light curve is characterized by an envelope of excess power consisting of a series of regular peaks (e.g. Fig. 1 in Kjeldsen et al. 2009). The oscillations are characterized by the frequency of maximum power (ν_{max}) and the large frequency separation ($\Delta\nu$). Here, $\Delta\nu$ is the separation between peaks with the same spherical degree (l) and consecutive radial order (n). In general, the large separation will vary slightly

with frequency but its mean value scales with the square root of mean density of the star (Ulrich 1986). Measured relative to the solar value the expression is (Kjeldsen & Bedding 1995):

$$\frac{\Delta\nu}{\Delta\nu_{\odot}} = \left(\frac{\rho}{\rho_{\odot}}\right)^{1/2} = \left(\frac{M}{M_{\odot}}\right)^{1/2} \left(\frac{R}{R_{\odot}}\right)^{-3/2}. \quad (1)$$

When the radius can be determined from interferometric measurements (combining angular diameter and parallax; see Sect. 4.1) we can determine the mass from this expression. We have compared the mass for the binary stars and from Eq. 1 for three stars (Procyon A and α Cen A+B) and the results agree very well, as is shown in the upper panel in Fig. 2. The mean relative difference is $\Delta M/M = +0.005 \pm 0.023$ (rms error). We also plot the comparison for 70 Oph A (also in a binary system) but in this case there is no published angular diameter and so the radius was derived from $R \propto L^{1/2} T_{\text{eff}}^{-2}$ (see Sect. 4.1). As a consequence, the mass of 70 Oph A has a much larger uncertainty (12%) than the three other binary stars (4.3–4.8%).

For 18 stars in our sample, $\Delta\nu$ has been measured. For four others, α For, γ Ser, β Aql and δ Pav, only ν_{max} has been measured. However, Kjeldsen & Bedding (1995) determined a scaling between $\Delta\nu$ and ν_{max} as

Table 2. Fundamental parameters of the 23 targets as determined from the methods or parameters given in parenthesis: $\langle \rangle$, e.g. binary orbit, asteroseismic information (ρ), interferometry (θ_{LD}), parallax (π_p), bolometric flux (f_{bol}), and spectroscopic analysis with VWA. Spectroscopic T_{eff} s are offset by -40 K as discussed in the text. The uncertainties on the spectroscopic and photometric T_{eff} s are 80 and 90 K, respectively, and 0.07 and 0.10 dex for $[Fe/H]$. Parameters from indirect methods are marked by the \star symbol.

Star	M/M_{\odot} (Binary orbit)	M^*/M_{\odot} (ρ, R)	R/R_{\odot} (θ_{LD}, π_p)	R^*/R_{\odot} (L, T_{eff})	L/L_{\odot} (f_{bol}, π_p)	L^*/L_{\odot} (V, BC, π_p)	T_{eff} [K] (θ_{LD}, f_{bol})	T_{eff}^* [K] (Spec.)	T_{eff}^* [K] (Phot.)	[Fe/H]* (Spec.)	[Fe/H]* (Phot.)
β Hyi		$^a 1.08 \pm 0.05$	1.810 ± 0.015	1.89 ± 0.06	3.41 ± 0.13	3.57 ± 0.11	5840 ± 59	5790	5870	-0.10	-0.04
τ Cet		$^a 0.79 \pm 0.03$	0.794 ± 0.005	0.85 ± 0.03	0.47 ± 0.02	0.50 ± 0.02	5383 ± 47	5290	5410	-0.48	-0.42
ι Hor		$^c 1.23 \pm 0.12$		1.16 ± 0.04		1.64 ± 0.05		6080	6110	+0.15	-0.00
α For		$^d 1.53 \pm 0.18$		2.04 ± 0.06		4.87 ± 0.16		6015	6105	-0.28	-0.16
δ Eri		$^a 1.33 \pm 0.07$	2.327 ± 0.029	2.41 ± 0.09	3.00 ± 0.12	3.26 ± 0.14	4986 ± 57	5015		+0.15	
α Men				0.99 ± 0.03		0.83 ± 0.03		5570	5580	+0.15	+0.07
Procyon A	1.461 ± 0.025	$^a 1.45 \pm 0.07$	2.059 ± 0.015	2.13 ± 0.06	6.77 ± 0.20	7.17 ± 0.22	6494 ± 48	6485	6595	+0.01	+0.02
171 Pup		$^c 0.99 \pm 0.11$		1.24 ± 0.04		1.46 ± 0.05		5710	5790	-0.86	-0.75
ξ Hya		$^b 2.89 \pm 0.23$	10.207 ± 0.111	10.14 ± 0.39	57.65 ± 2.39	59.38 ± 2.58	4984 ± 54	5045		+0.21	
β Vir		$^a 1.42 \pm 0.08$	1.704 ± 0.022	1.69 ± 0.05	3.40 ± 0.12	3.40 ± 0.10	6012 ± 64	6050	6150	+0.12	+0.10
η Boo		$^a 1.77 \pm 0.11$	2.701 ± 0.040	2.66 ± 0.09	8.65 ± 0.35	8.66 ± 0.36	6028 ± 47	6030	6025	+0.24	+0.27
α Cen A	1.105 ± 0.007	$^a 1.14 \pm 0.05$	1.225 ± 0.004	1.24 ± 0.04	1.47 ± 0.05	1.51 ± 0.05	5746 ± 50	5745	5635	+0.22	+0.12
α Cen B	0.934 ± 0.006	$^a 0.92 \pm 0.04$	0.864 ± 0.005	0.91 ± 0.03	0.47 ± 0.02	0.51 ± 0.02	5140 ± 56	5145		+0.30	
HR 5803		$^c 1.52 \pm 0.16$		1.56 ± 0.05		3.23 ± 0.14		6200	6280	-0.04	-0.11
γ Ser		$^d 1.30 \pm 0.15$		1.55 ± 0.05		3.02 ± 0.09		6115	6245	-0.26	-0.19
μ Ara		$^c 1.21 \pm 0.13$		1.39 ± 0.05		1.78 ± 0.06		5665	5690	+0.32	+0.19
70 Oph A	0.890 ± 0.020	$^c 1.10 \pm 0.13$		0.91 ± 0.03		0.59 ± 0.02		5300		+0.12	
η Ser		$^d 1.45 \pm 0.21$		6.10 ± 0.25		18.32 ± 0.87		4850		-0.11	
β Aql		$^b 1.26 \pm 0.18$	3.211 ± 0.133	3.30 ± 0.12	5.73 ± 0.19	6.23 ± 0.25	4986 ± 111	5030		-0.21	
δ Pav		$^d 1.07 \pm 0.13$		1.20 ± 0.04		1.22 ± 0.04		5550	5540	+0.38	+0.33
γ Pav		$^c 1.21 \pm 0.12$		1.15 ± 0.04		1.52 ± 0.05		5990	6135	-0.74	-0.57
τ PsA		$^c 1.34 \pm 0.13$		1.45 ± 0.04		2.82 ± 0.09		6235	6385	+0.01	+0.05
ν Ind		$^d 1.00 \pm 0.13$		3.18 ± 0.12		6.28 ± 0.23		5140		-1.63	

Notes on column 3: (a): Mean density, ρ , is scaled from $\Delta\nu$; radius, R , is from interferometry. (b): ρ is scaled from ν_{max} ; R is from interferometry. (c): ρ is scaled from $\Delta\nu$; R is from $R \propto L^{1/2} T_{eff}^{-2}$. (d): ρ is scaled from ν_{max} ; R is from $R \propto L^{1/2} T_{eff}^{-2}$.

$$\frac{\Delta\nu}{\Delta\nu_{\odot}} = \left(\frac{\nu_{max}}{\nu_{max;\odot}} \right)^{1/2} \left(\frac{R}{R_{\odot}} \right)^{1/2} \left(\frac{T_{eff}}{T_{eff;\odot}} \right)^{1/4}. \quad (2)$$

We used this expression using the radius from Sect. 4.1 and T_{eff} from the spectroscopic analysis (Sect. 5). A comparison with the more recent $\Delta\nu - \nu_{max}$ calibration of Stello et al. (2009) shows agreement within 1σ for all four stars.

In Table 1 we give a list of the values of $\Delta\nu$ and ν_{max} from the literature. The quality and quantity of the data sets used for the determination of these asteroseismic values span a wide range. Some data sets are single-site observations lasting one night while in one case (Procyon A), a multi-site campaign was carried out using 11 telescopes lasting three weeks. In addition, some stars have been observed more than once. It would be difficult to give a homogeneous set of uncertainties, so instead we adopted uncertainties on $\Delta\nu$ and ν_{max} of 2 and 5%, respectively. To determine the mass as described above, we used $\Delta\nu$ if it is available, otherwise we used ν_{max} . In the case of the two most evolved stars (ξ Hya and η Ser) the large separation is 7–8 μ Hz. It is well-known that it requires long time-series to be able to resolve the individual peak for evolved stars. For this reason we adopted the more robust value of ν_{max} for these two stars (see also Stello et al. 2009).

The determined masses of the 22 stars with asteroseismic information available are given in column 3 in Table 2. Four different combinations were used to determine the mean density (either Eq. 1 or 2) and the radius (from interferometry or the relation $R \propto L^{-1/2} T_{eff}^{-2}$; see Sect. 4.1). The combination used for each star is explained below Table 2. The propagation of errors yield uncertainties in the range 4–15%.

We emphasize that our mass estimates rest on the assumption of the absolute validity of the scaling relations of Eq. 1 and 2. The uncertainty estimate we give here comes only from the error propagation of $\Delta\nu$, ν_{max} and R (and also T_{eff} for Eq. 2). The absolute values of the masses but also the uncertainties will require a more extensive study and the results given here should therefore be used with caution.

2.3 Accuracy of single-star masses

Using the same approach that we adopted in Sect. 2.2, North et al. (2007) analysed β Hyi and Teixeira et al. (2009) analysed τ Cet. They obtained masses of $1.07 \pm 0.03 M_{\odot}$ and $0.783 \pm 0.012 M_{\odot}$, respectively. For β Hyi, Kjeldsen et al. (2008) corrected the asteroseismic data for surface effects and used the updated *Hipparcos* parallax to obtain $1.085 \pm 0.028 M_{\odot}$. We used nearly the same data so it is not surprising that our values are almost identical: 1.08 ± 0.05 and $0.79 \pm 0.03 M_{\odot}$. The reason for the higher uncertainties is that we assumed a common (larger) uncertainty on the large separation.

We will now compare our estimates with three studies that combine asteroseismic information (large separation or individual oscillation frequencies) and classical constraints. In these studies, the classical constraints include a spectroscopic T_{eff} and metallicity and the luminosity is determined from the V magnitude and parallax while adopting a bolometric correction to obtain the bolometric flux (as described in Sect. 4.2).

The sub-giant η Boo was analysed by Guenther et al. (2005) based on direct modelling of the individual oscillation frequencies.

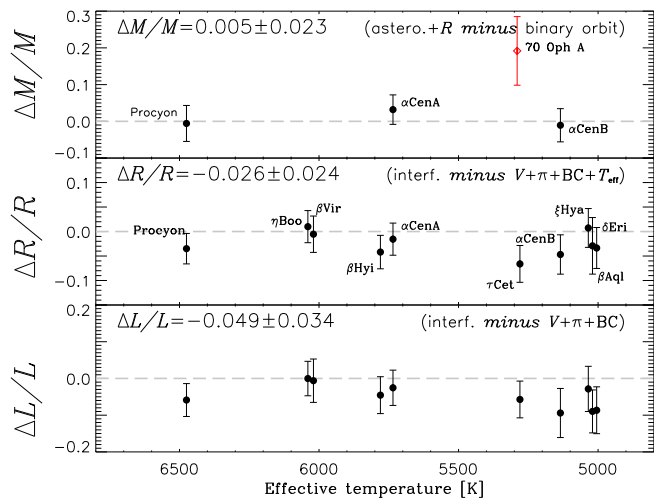


Figure 2. Relative differences between fundamental parameters as determined by direct and indirect methods (cf. Table 2). In the top panel 70 Oph A is marked by an open symbol since its radius is determined from an indirect method and is therefore more uncertain. The effective temperature on the abscissa is the spectroscopic value.

They determined a mass of $1.71 \pm 0.05 M_{\odot}$, in good agreement with our value of $1.77 \pm 0.11 M_{\odot}$. The main sequence star ι Hor was modelled by Vauclair et al. (2008). They considered different values for the helium content and metallicity and determined a very precise mass $1.25 \pm 0.01 M_{\odot}$, which agrees with our less precise estimate of $1.15 \pm 0.12 M_{\odot}$. Bedding et al. (2006) determined a mass $0.85 \pm 0.04 M_{\odot}$ for the population-II sub-giant ν Ind. They constrained the location in the H-R diagram using both classical constraints ($L/L = 6.21 \pm 0.23$ and $T_{\text{eff}} = 5300 \pm 100$ K) and asteroseismic information (the large separation). They used model grids for different overshoot parameters but with a fixed metallicity at $Z = 0.001$. Our mass determined from the simple scaling is $1.05 \pm 0.12 M_{\odot}$ and is in agreement with Bedding et al. (2006).

The excellent agreement with the 4 stars with direct binary masses (top panel in Fig. 2) and the good agreement for 3 detailed model-comparisons discussed above give us confidence in the method we adopted. Although the uncertainties are relatively large, they offer a starting point for more detailed modelling, which can potentially lead to more accurate estimates of the mass and age.

3 DIRECT MEASUREMENTS: θ , π_p AND f_{bol}

3.1 Angular diameters

The angular diameters of stars can be measured using interferometry and can be used to infer nearly model-independent linear radii and effective temperatures (see Sect. 4.1 and 4.4). The observations consist of measuring fringe visibility as a function of baseline. The usual approach is to fit the observed visibilities with a uniformly illuminated disk and to convert the diameter to a limb-darkened (LD) disk using correction factors from atmospheric models. This is the approach used for the LD diameters taken from the literature and given in Table 2 for ten stars. However, we note that for more extended baselines with visibilities measured beyond the first null, a direct fit including the limb-darkening is needed (e.g. as done for Procyon A by Aufdenberg et al. 2005).

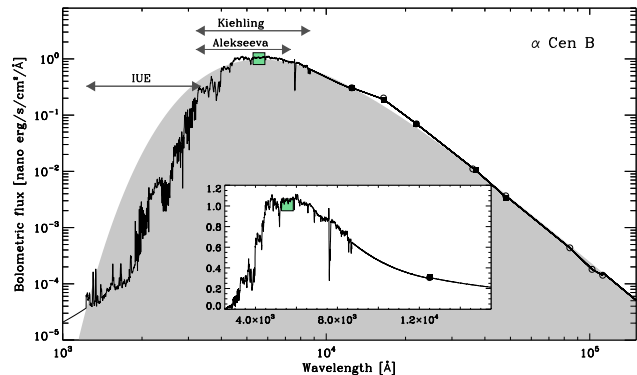


Figure 3. The bolometric flux of α Cen B is determined by integrating the black curve shown here. The ranges for the satellite IUE data and the spectrophotometric data are indicated by arrows and the name of the first author. Box symbols and circles are broad-band fluxes. The inset shows the details in the visual range on a linear scale.

Allende Prieto et al. (2002) discussed the case of Procyon A and in particular the difference between plane-parallel 1D and 3D hydrodynamical models. They found that their 3D model results in a slightly smaller LD correction factor, resulting in smaller linear radii (1.6%) and thus a higher effective temperature (50 K). Bigot et al. (2006) used a 3D model to infer the limb darkening parameter of the much cooler star α Cen B. They also found a slightly smaller linear radius (0.3%) compared to their 1D model. When comparing these results for 1D and 3D models it is important to note that Allende Prieto et al. (2002) used the angular diameter measured in the visible (Mozurkewich et al. 1991) and Bigot et al. (2006) used infrared interferometric data. This may partly explain the difference between the studies (see also Aufdenberg et al. 2005), and future studies of other solar-type stars will shed more light on this issue.

For simplicity and uniformity we shall use the limb-darkened diameters (θ_{LD}) from the literature based on 1D LTE models as originally published (for further discussion see Sect. 4.4) and listed in Table 1. In some cases more than one angular diameter exists and we have computed the weighted mean value, as done by Teixeira et al. (2009) for τ Cet.

3.2 Bolometric fluxes

The bolometric flux (f_{bol}) can be estimated using UV measurements from space, spectrophotometry in the visible region, and broadband magnitudes in the near infrared. Since the target stars are nearby we neglect interstellar absorption¹.

We used UV spectrophotometry (1150–3350 Å) from the International Ultraviolet Explorer (IUE²). Several dozen spectra are available for most stars except α Men, β Vir, η Boo, and β Aql, where fewer than ten were available. For ξ Hya no IUE data are available and we used the broadband UV data from the Ultraviolet Sky Survey Telescope on the TD-1 satellite (Thompson et al. 1978). In the visual regime we used spectrophotometry from Breger (1976), Kiehling (1987) and Alekseeva et al. (1996). In the near-IR and IR we used broadband photometry from Morel & Magnenat

¹ All 23 stars are closer than 40 pc, and 20 stars are closer than 20 pc.

² The IUE spectra are available from <http://sdc.laeff.inta.es/ines/>.

(1978), Thomas et al. (1973), and Engels et al. (1981). For the broadband data we calculated absolute fluxes using the values for Vega listed in Cox (2000). For a few targets we used additional flux values from the *COBE* DIRBE point source catalog (Smith et al. 2004).

An example of the available data for α Cen B is shown in Fig. 3. It comprises UV data from the IUE satellite, spectrophotometric data from Kiehling (1987) and broadband photometry from Engels et al. (1981) (squares) and Thomas et al. (1973) (circles). The grey shaded area is the Planck black body curve for the determined T_{eff} after scaling by using the angular diameter.

The measured fluxes are listed in Table 1 (column 6). We find good agreement with previous determinations of f_{bol} in the literature. For β Hyi, North et al. (2007) found $2.019 \pm 0.050 \text{ nW m}^{-2}$, compared to our value of $1.970 \pm 0.073 \text{ nW m}^{-2}$. For β Vir, North et al. (2009) found $0.944 \pm 0.020 \text{ nW m}^{-2}$ and we have $0.915 \pm 0.032 \text{ nW m}^{-2}$. Fuhrmann et al. (1997) combined several estimates in the literature for Procyon A to get a mean value of $18.20 \pm 0.43 \text{ nW m}^{-2}$ where we get 17.60 ± 0.48 . For these three stars our f_{bol} values are all lower but agree with the literature values within 1σ .

3.3 *Hipparcos* parallaxes

We used the updated *Hipparcos* parallaxes (π_{p}) from van Leeuwen (2007) and listed in Table 1. The values agree well with the originally published results Perryman et al. (1997) for all stars, but in one case the uncertainty is lower by a factor 4. This is for the giant star ξ Hya where the original value is $\pi_{\text{p}} = 72.95 \pm 0.83 \text{ mas}$ and the new value is $\pi_{\text{p}} = 73.00 \pm 0.20 \text{ mas}$. This means that the uncertainty on the linear radius decreases significantly from 3.4 to 1.0%. For the binary pair α Cen A+B we used the parallax from Söderhjelm (1999) since this analysis takes into account the binary orbit.

4 INDIRECT ESTIMATES OF R , L AND T_{eff}

4.1 Radius

The linear radius is determined from the limb darkened angular diameter and the parallax through the relation

$$R/R_{\odot} = 9.30 \times 10^{-3} \theta_{\text{LD}}/\pi_{\text{p}}, \quad (3)$$

where we use values of θ_{LD} and π_{p} in milliarcseconds (mas) from Table 1. The resulting linear radii are given in column 4 in Table 2. The uncertainties on R range from 0.2% (α Cen A) to 4% (β Aql).

For 13 stars without measured angular diameters we estimated the radius from the relation $R/R_{\odot} = (L/L_{\odot})^{1/2} (T/T_{\text{eff},\odot})^{-2}$. We have used indirect estimates for L and T_{eff} : L is found using the V magnitude, bolometric correction and parallax (Sect. 4.2) and T_{eff} is from the spectroscopic analysis (Sect. 4.4). We obtain radii with a *precision* of about 2–4% from this method.

The direct and indirect estimates of the radius are compared in the middle panel in Fig. 2. There is very good agreement for all ten stars, with the largest deviation being $7 \pm 4\%$ for τ Cet. The mean relative difference of $\Delta R/R = -0.022 \pm 0.024$ (rms error) indicates that the claimed precision is realistic. Since we have a significant number of stars we propose that the indirect method is *accurate* with a $1\text{-}\sigma$ uncertainty of $\approx 3\%$.

4.2 Luminosity

The luminosity can be determined directly from the bolometric flux (f_{bol}), and the parallax (π_{p}) through

$$L/L_{\odot} = 3.12 \times 10^4 f_{\text{bol}} / \pi_{\text{p}}^2, \quad (4)$$

where we insert the values of f_{bol} and π_{p} from Table 1 in units of nW and mas , respectively. The resulting luminosities are given in column 6 in Table 2.

In Sect. 3.2 we described how we determined f_{bol} for ten stars. The parallax is available from van Leeuwen (2007) for all targets. We have compared the resulting L with an indirect method that relies on the apparent V magnitude, bolometric correction (see Sect. 4.3) and the parallax. The bolometric magnitude is defined as $M_{\text{bol}} = V + \text{BC}_V + 5 \log \pi_{\text{p}} + 5$. We assumed that the interstellar reddening is zero since all targets are relatively close. We obtained V from SIMBAD and adopted the uncertainty $\sigma(V) = 0.015$. We converted M_{bol} to L/L_{\odot} using $M_{\text{bol},\odot} = 4.75 \pm 0.01$ (IAU recommendation 1999).

In the bottom panel in Fig. 2 the values are compared to the luminosity determined for ten stars combining the angular diameter with the parallax (Eq. 4). The mean relative difference is $\Delta L/L = -0.048 \pm 0.033$ (rms error), indicating there is little or no systematic error. The largest deviations are $9 \pm 6\%$ for the three cool stars α Cen B, β Aql and δ Eri. In fact, all five stars with T_{eff} below 5300 K appear to have overestimated luminosities from the indirect method, indicating that their BCs are too negative (Fig. 4 shows that BCs change rapidly for cool temperatures). We note that adding 0.03 mag to all BCs would make the indirect luminosities and radii agree with the direct measures to within $1\text{-}\sigma$ for all ten stars. The mean relative differences would then improve to $\Delta L/L = -0.020 \pm 0.034$ and $\Delta R/R = -0.010 \pm 0.027$.

From the comparison between the direct and indirect methods we conclude that the luminosity can be determined to $\approx 3\%$ from $V + \pi_{\text{p}} + \text{BC}$. The values are listed for all 23 stars in column 7 in Table 2. We caution that we find evidence for a slight overestimation of L from the indirect method for cool stars.

4.3 Bolometric correction

We have investigated the differences between some commonly used tabulations of bolometric corrections (BC), i.e. from Flower (1996), Bessell et al. (1998), Girardi et al. (2002) and Vandenberg & Clem (2003). For Girardi et al. we used the updated results from the dustyAGB07 database³. The BC values in these works are all based on atmospheric models and have slightly different dependencies, as shown in Fig. 4. The BCs from Flower (1996) only depend on T_{eff} , while Bessell et al. (1998) values include a slight dependency with $\log g$. Both Vandenberg & Clem (2003) and Girardi et al. (2002) include the changes in BC with $\log g$ and $[\text{Fe}/\text{H}]$. This has an important impact on the BC for the metal-poor stars in our sample (τ Cet, 171 Pup, γ Pav and ν Ind). In Fig. 4 we show the difference between $[\text{Fe}/\text{H}] = 0.0$ and -1.0 for Girardi et al. (2002) and Vandenberg & Clem (2003). For these two studies, the mean difference of the BCs for the 23 stars is negligible, $\Delta \text{BC} = +0.007 \pm 0.019$ (rms error).

Inspecting the four tabulations of BC for $[\text{Fe}/\text{H}] = 0.0$ and $\log g = 4.5$ in Fig. 4, we find the maximum difference is about 0.04 mag in the range 5000–6500 K. Based on this we assign a $1\text{-}\sigma$

³ <http://stev.oapd.inaf.it/dustyAGB07/>.

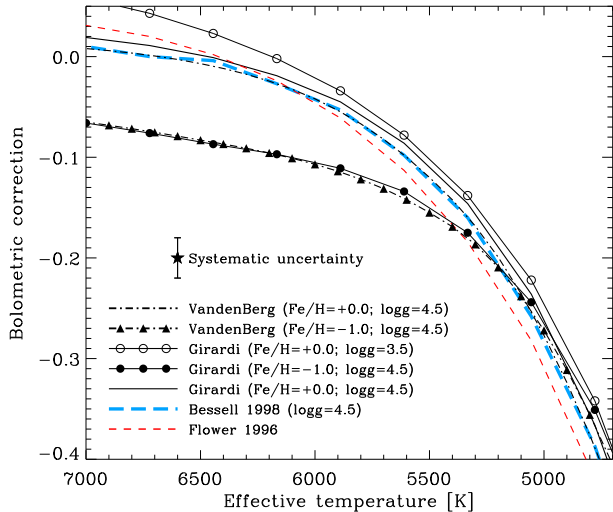


Figure 4. Bolometric corrections from four different sources. We have adopted the BCs from VandenBerg & Clem (2003) that take into account the changes with metallicity and $\log g$.

systematic uncertainty of 0.02 mag to the BC. We note that the BC tabulations we have compared depend on their adopted metallicity scale relative to the Sun. However, recent studies of the metallicity of the Sun indicate a lower value than previously thought (mostly due to revision of the light elements C and O; Caffau et al. 2008). This could mean that the opacities used for the calculation of the BCs include some bias, especially above 5500 K, where Fig. 4 shows that metallicity plays an important role.

In the following we have adopted the tabulations of VandenBerg & Clem (2003) and the BC values are interpolated in their grids. We included the uncertainties on T_{eff} (80 K), $\log g$ (0.08 dex) and $[\text{Fe}/\text{H}]$ (0.07 dex) to determine the BC for each star with an uncertainty of 0.03 mag. The values for the atmospheric parameters (T_{eff} , $\log g$ and $[\text{Fe}/\text{H}]$) are taken from the spectroscopic analysis in Sect. 5. The BC values are given in Table 1 (column 7).

4.4 Effective temperatures

The effective temperature can be directly determined from the limb-darkened angular diameter and the bolometric flux from the definition

$$\sigma T_{\text{eff}}^4 = 4 f_{\text{bol}} / \theta_{\text{LD}}^2, \quad (5)$$

where σ is the Stefan-Boltzmann constant. Eq. 5 can also be expressed as

$$T_{\text{eff}} = 7402 \times f_{\text{bol}}^{0.25} / \theta_{\text{LD}}^{0.5}, \quad (6)$$

where the unit of f_{bol} is nW and θ_{LD} is in mas as given in Table 1. In Table 2 we list the T_{eff} determined for the ten stars with measured angular diameters (column 8).

We used two indirect methods to determine T_{eff} . One is based on detailed spectroscopic analysis of Fe I and II lines using high-quality spectra and is described in Sect. 5. The second method is based on Strömgren photometric indices with the recent calibration by Holmberg et al. (2007). This calibration is not valid for the most evolved stars in the sample. We used indices from the homo-

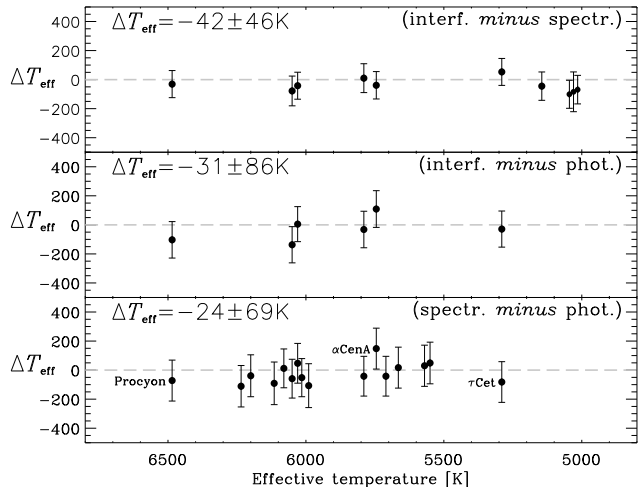


Figure 5. Differences between T_{eff} determined by direct and indirect methods (cf. Table 2): angular diameter and bolometric flux (“interf.”), spectroscopic determination (“spectr.”), and Strömgren photometric indices (“phot.”). The effective temperature on the abscissa is the spectroscopic value.

geneously calibrated catalogue of E. H. Olsen⁴ (Olsen 1994). We determined T_{eff} from the Holmberg et al. (2007) calibration for 16 stars. The spectroscopic and photometric T_{eff} s are given in columns 9 and 10 in Table 2.

The three methods are compared in Fig. 5. There is very good agreement between the methods and the deviation is below 1σ for most stars. This indicates that the uncertainties are slightly overestimated. The spectroscopic and interferometric T_{eff} have a mean offset of -42 ± 46 K (rms error; ten stars). This indicates a slight systematic offset which we round off to -40 ± 20 K (error on the mean value). The interferometric and photometric T_{eff} have a mean offset of -31 ± 86 K (rms error; 6 stars). Finally, comparing the spectroscopic and photometric data we find a mean difference of -24 ± 69 K (rms error; 16 stars). A further examination of the Holmberg et al. (2007) calibration was done by Holmberg et al. (2009). They compared T_{eff} from the photometric calibration with interferometric and spectroscopic methods and the infrared flux method. They found good agreement with mean offsets no larger than 55 K.

Accurately calibrated Strömgren data is extremely useful for faint targets or large ensembles of stars when it is not feasible to collect a high quality spectrum of each star. However, interstellar reddening is often a limiting factor on the accuracy. To estimate the uncertainty on the photometric T_{eff} we used the calibration error (60 K; Holmberg et al. 2007) and assumed errors of 0.005 mag on $b - y$ and 0.07 dex of $[\text{Fe}/\text{H}]$. This gives an internal precision of about 70 K. From the comparison with interferometric T_{eff} we find an rms scatter of about 90 K, which we assign as the accuracy of the photometric T_{eff} s. To have an idea of the uncertainty when reddening becomes important, we increased the error on $b - y$ to 0.015 mag. The resulting internal uncertainty on the T_{eff} increase from 70 K to 115 K.

We have compared our T_{eff} using the direct method with results from the literature for five stars: Procyon A ($T_{\text{eff}} = 6512 \pm$

⁴ The complete “EHO” catalogue of more than 30 000 stars was obtained by private communication.

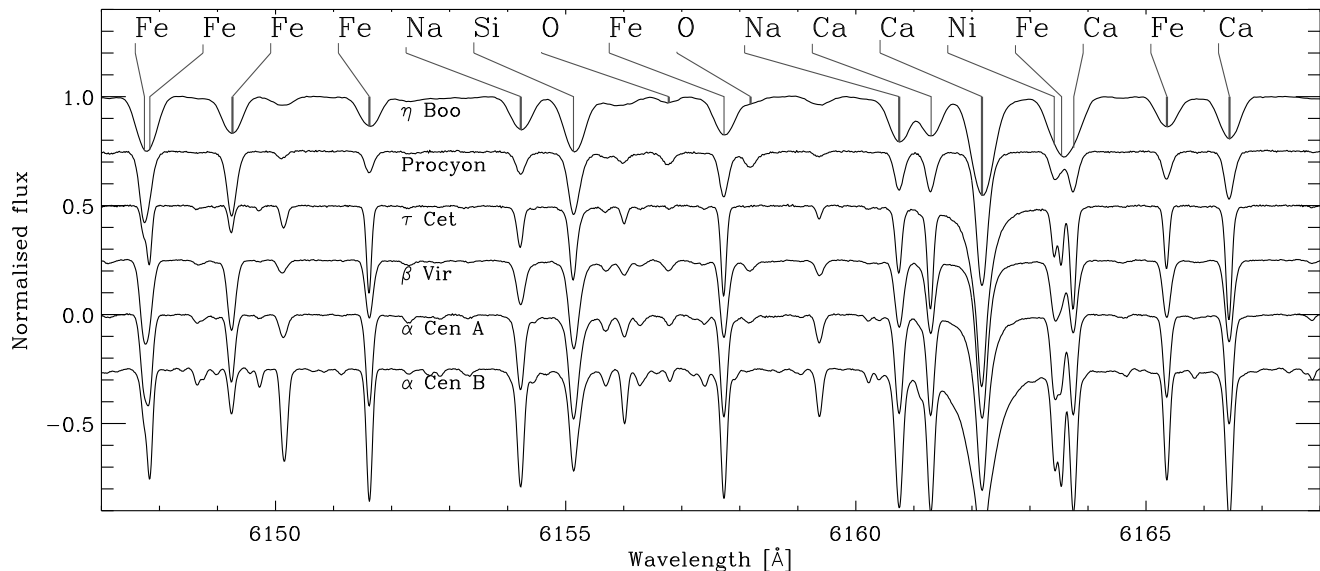


Figure 6. A small section of the observed spectra of six stars. These data represent 1% of the entire spectral range used to determine T_{eff} , $\log g$, $v \sin i$, and the chemical composition. The wide Ca line at $\lambda 6162 \text{ \AA}$ is used to constrain the $\log g$ value.

49 K; Allende Prieto et al. 2002), β Hyi ($T_{\text{eff}} = 5872 \pm 44 \text{ K}$; North et al. 2007), β Vir ($T_{\text{eff}} = 6059 \pm 49 \text{ K}$; North et al. 2009), η Boo ($T_{\text{eff}} = 6100 \pm 28 \text{ K}$; van Belle et al. 2007), and τ Cet ($T_{\text{eff}} = 5400 \pm 100 \text{ K}$; di Folco et al. 2007). We find slightly lower values of T_{eff} with the mean difference being $\Delta T_{\text{eff}} = -37 \pm 22 \text{ K}$ (rms error).

Although we have called the application of Eq. 6 a “direct method”, in fact θ_{LD} depends on the adopted limb-darkening coefficient, which does rely on models. As mentioned in Sect. 3.1, differences between 1D and 3D models yield a difference of 50 K for Procyon A (Allende Prieto et al. 2002) while for α Cen B it is negligible. Another complication is our assumption of zero interstellar reddening, which certainly will not hold for more distant stars. di Folco et al. (2007) found IR excess around τ Cet, which is one of our targets. They found the flux in the visible region to be well-fitted by a model with $T_{\text{eff}} = 5400 \pm 100 \text{ K}$, which agrees with our more simple assumptions resulting in $5383 \pm 47 \text{ K}$. We have estimated that the uncertainty on T_{eff} from the measurement errors (f_{bol} and θ_{LD}) is typically $\sigma_{\text{fund}} = 50\text{--}60 \text{ K}$ (although for β Aql it is $\approx 110 \text{ K}$). We estimate that the systematic uncertainty on T_{eff} (e.g. from using 1D and not 3D models) is probably about $\sigma_{\text{1D-3D}} = 50 \text{ K}$.

For our final set of homogeneously determined T_{eff} values, we have adopted the results from the spectroscopic analysis of 23 stars (see Sect. 5) but we apply the determined mean offset of $-40 \pm 20 \text{ K}$. The offset is valid for stars of spectral type F5–K2 with luminosity class III to V. The value is rounded off to 40 K for simplicity and the error on the mean is $\sigma_{\text{spec}} = 20 \text{ K}$ from ten stars. We have added the uncertainties as $\sigma^2 = \sigma_{\text{fund}}^2 + \sigma_{\text{1D/3D}}^2 + \sigma_{\text{spec}}^2 = (60^2 + 50^2 + 20^2) \text{ K}^2$, giving $\sigma = 80 \text{ K}$.

The relatively small scatter on the difference between T_{eff} from interferometry and spectroscopy gives us confidence that we can determine the T_{eff} to 80 K (1- σ uncertainty). From a high-quality spectrum, this should be possible to achieve for any late-type star. We mention that the Versatile Wavelength Analysis method (VWA; see Sect. 5.2) has already been used in the spectroscopic study of several targets of *CoRoT* (Bruntt 2009) and *Kepler*

(Chaplin et al. 2010). However, in these studies the -40 K offset was not known, but we recommend that it is applied.

5 SPECTROSCOPIC ANALYSIS

We used high-resolution high-S/N spectra to determine the atmospheric parameters of the stars: T_{eff} , $\log g$, chemical composition, and $v \sin i$. This is a well-known and widely used “classical” analysis method (Fuhrmann 1998; Valenti & Fischer 2005), but it is indirect since it relies on the adopted model atmospheres. In this Section, we will determine the chemical composition in the photosphere, which provides important input to asteroseismic modelling. Also, we will compare the detailed analysis with the metallicity determined from Strömberg indices. Finally, we have analysed non-blended lines to determine the line broadening due to $v \sin i$ and macroturbulence.

5.1 Spectroscopic observations

We used spectra of the 23 targets, primarily from the High Accuracy Radial velocity Planet Searcher (HARPS spectrograph; $R = 115\,000$) mounted on the ESO 3.6 m telescope at La Silla, Chile. The exceptions are the spectrum of β Hyi from the University College of London Echelle Spectrograph (UCLES; $R = 65\,000$) at the 3.9 m Anglo-Australian Telescope and the spectrum of η Boo from the Fibre-fed Echelle Spectrograph (FIES; $R = 68\,000$) at the 2.5 m Nordic Optical Telescope. In most cases the spectra have been observed as part of asteroseismic campaigns, which means several hundred spectra are available in some cases. We selected typically 20–60 spectra of each target, collected on the same night, and these were co-added after discarding spectra with poor S/N. The S/N of the spectra was calculated in continuum windows in the range 5800–6200 \AA , with typical values from 400–800. In Fig. 6 we show examples of spectra for six of the target stars. Although the shown spectral range contains rich information, it comprises only 1% of the entire available range. The wide Ca line at

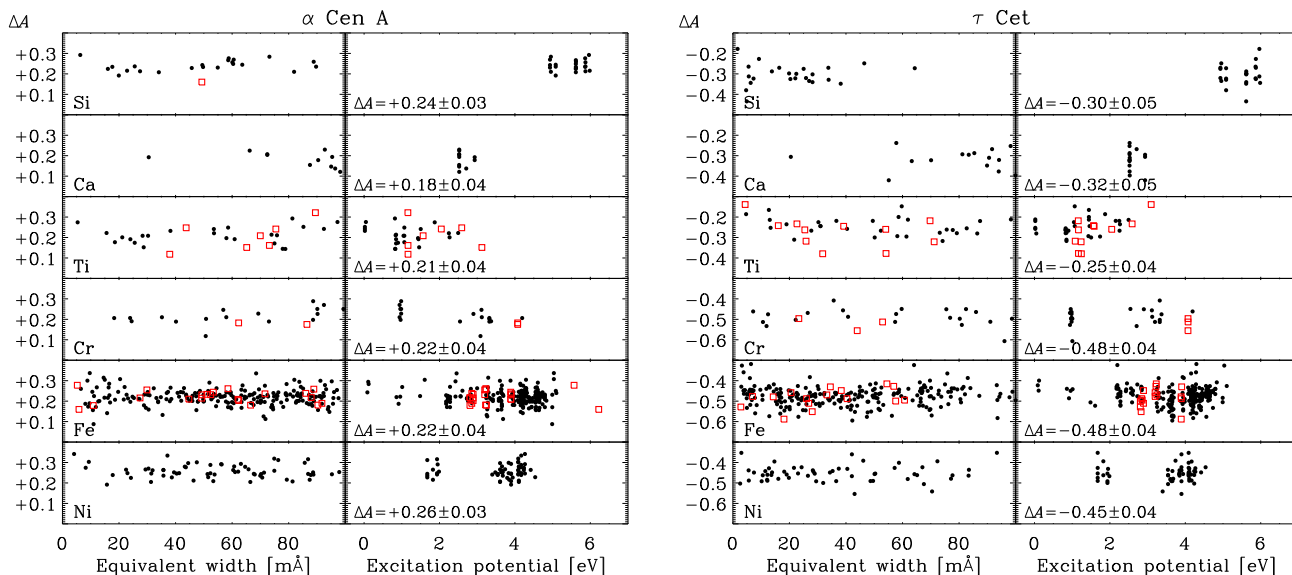


Figure 7. Abundances relative to the Sun for six atomic species in α Cen A and τ Cet. The abundances are plotted versus equivalent width and excitation potential and no significant correlations are seen, indicating that the atmospheric model parameters are correct. The mean abundances and rms scatter determined from the neutral lines are given in the right panels as ΔA . Neutral and singly ionized lines are marked with filled and open symbols, respectively. Notice the enhancement of about 0.2 dex for the α elements (Si, Ca, Ti) in the metal-poor star τ Cet.

$\lambda 6162 \text{ \AA}$ is one of the indicators used to constrain the surface gravity (Sect. 5.3).

We used pipeline-reduced spectra which in most cases automatically merges the overlapping echelle orders. For this reason we chose not to use the Balmer lines, although they could be used to constrain T_{eff} for the early-type stars in the sample. The spectra from the pipeline were normalized by identifying continuum windows in the spectrum. This was done manually by comparing the observed spectrum with a template spectrum computed with the same approximate parameters (T_{eff} , $\log g$, $[\text{Fe}/\text{H}]$, and $v \sin i$) as the observed star. The template was very useful for identifying “true” continuum windows or regions where the rectification of the spectrum cannot be done objectively. For a detailed description of the rectification process we refer to Bruntt, Fridlund & Deleuil (2010, A&A, submitted).

The abundance analysis was based on 1D atmospheric MARCS models (Gustafsson et al. 2008) that assume local thermodynamic equilibrium (LTE). We used atmosphere models interpolated in a grid and atomic line data are from VALD (Kupka et al. 1999). For the region around lithium at $\lambda 6707.8 \text{ \AA}$, we used atomic data from Ghezzi et al. (2009), although we did not include the weak CN bands. The model atmospheres used the recently revised Solar abundances (Grevesse et al. 2007) and included α -element enhancement for metal-poor stars. To correct for the short-comings of the 1D LTE analysis to first order, we measured abundances differentially with respect to a Solar spectrum (see Bruntt et al. 2008). However, we caution that some elements will be affected by non-LTE effects, especially for cool and low-metallicity stars (for a discussion, see Asplund 2005). Our reference spectrum was taken from the book by Hinkle et al. (2000) (published in original form by Kurucz et al. 1984). This spectrum was acquired with the Fourier Transform Spectrometer (FTS) on the McMath Solar Telescope at Kitt Peak National Observatory.

The design of the FTS ensures that there is no scattered light. However, our observations were made with three different echelle

spectrographs that could potentially be affected by scattered light. For the FIES spectrum of η Boo we found Fe I abundances to be ≈ 0.1 dex lower for lines with wavelengths shorter than 5500 \AA . This could be an indication for the presence of scattered light or improper subtraction of the flux between the closely spaced echelle orders at short wavelengths. A similar effect was seen for the UCLES spectrum of β Hyi. For this reason we only used spectral lines above 5500 \AA for η Boo and β Hyi. The effect was not seen in the HARPS spectra and so the entire spectral range was used.

5.2 T_{eff} , $\log g$, microturbulence from iron lines

We used the VWA software (Bruntt et al. 2004, 2008; Bruntt 2009) to analyse the spectra. This semi-automatic software package selects the least blended lines and iteratively fits the abundances. Lines were selected for each star and the fit of the synthetic spectrum was carefully investigated. Typically, 600–1000 lines could be used, although for the relatively fast rotators (τ PsA, η Boo and γ Ser) we used 250–400 lines. The part of spectrum with most of the lines ranged from 4880 to 6820 \AA , while we generally avoided regions affected by telluric lines (e.g. 5880 – 6000 and 6275 – 6330 , and 6460 – 6600 \AA). We initially used a model atmosphere with $\log g$ and T_{eff} as determined from the spectral type and solar metallicity was assumed. The atmospheric parameters and the microturbulence were then refined in several steps. This was done by minimizing the correlations between the abundance of Fe I lines and equivalent width and excitation potential, and requiring good agreement between the abundances of the neutral and ionized species of Fe, Cr and Ti.

As examples of the quality of the data, we show the abundance of Si, Ca, Ti, Cr, Fe and Ni for α Cen A and τ Cet in Fig. 7. The mean abundance and rms scatter are indicated in the right panels for the neutral lines. It is seen that the metal-poor star τ Cet has a relatively high abundance of the α -elements (Si, Ca, and Ti) compared to the other metals.

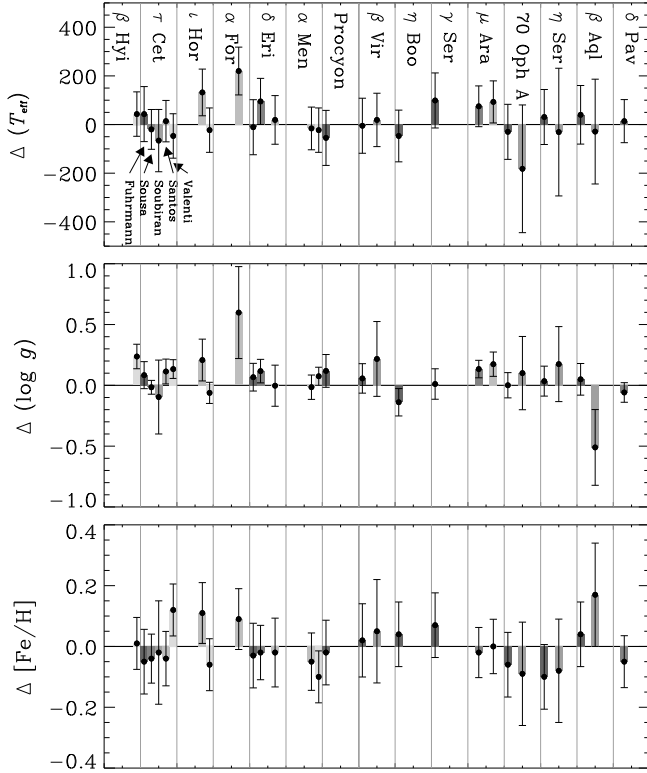


Figure 8. Atmospheric parameters from five studies in the literature compared to values from VWA. Individual values are given in Appendix A.

One of the best-studied solar-type stars is α Cen A and Porto de Mello et al. 2008 provided a list of 17 studies. Among the 13 that were based on spectroscopic data there is very good agreement on T_{eff} and $\log g$, and most studies indicate $[\text{Fe}/\text{H}] \approx +0.25$. The two most detailed studies of α Cen A are those of Neuforge-Verheecke & Magain (1997) and Porto de Mello et al. (2008) who adopted a differential analysis similar to ours. Their results for the spectroscopic parameters agree with ours, but we include 3–6 times as many spectral lines. While this allows us to derive the atmospheric parameters with lower intrinsic error, it is the systematic errors that dominate the uncertainty.

Several of the targets have been analysed using similar techniques in the literature. As a consistency check we have compared the atmospheric parameters with similar recent studies that also use 1D LTE models and similar recipes for adjusting T_{eff} , $\log g$ and microturbulence. In Fig. 8 we compare our T_{eff} , $\log g$ and $[\text{Fe}/\text{H}]$ with five studies indicated by the gray bars. From left to right it is Fuhrmann (1998, 2004, 2008), Sousa et al. (2008), Soubiran et al. (1998), Santos et al. (2004, 2005), and Valenti & Fischer (2005). In Appendix A we list the values from the literature. The maximum deviations are 220 K in T_{eff} , 0.58 dex in $\log g$, and 0.24 dex in $[\text{Fe}/\text{H}]$. These are quite large deviations compared to the typical uncertainties we have determined. However, for the most deviant parameters, the literature nearly always quote large uncertainties. For the $\log g$ of α For, Santos et al. (2004) found 4.40 ± 0.37 while we have 3.82 ± 0.08 . The high $\log g$ value explains the high T_{eff} found by Santos et al. (2004) ($\Delta T_{\text{eff}} = 220$ K), since $\log g$ and T_{eff} are not independent. For the $\log g$ of β Aql, Soubiran et al. (1998) found 3.04 ± 0.30 where we get 3.61 ± 0.08 in agreement with Fuhrmann (2004) who found 3.60 ± 0.10 . For the same star, Soubiran et al. (1998) found $[\text{Fe}/\text{H}] = -0.04 \pm 0.15$, while we

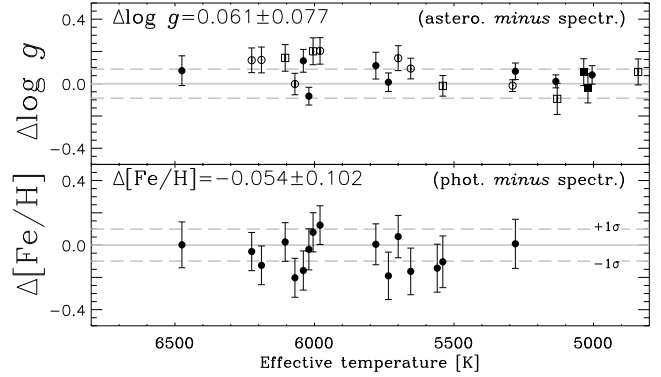


Figure 9. Top panel: Difference in $\log g$ determined from asteroseismic information and spectroscopic analysis. Solid symbols are used for stars with measured angular diameters. Bottom panel: Difference in metallicity determined from Strömgren indices and spectroscopic determination. The individual values are given in Table 2 and 3.

find -0.20 ± 0.07 , which is in agreement with Fuhrmann (2004) who found -0.17 ± 0.07 .

We conclude that our spectroscopic analysis is in good agreement with previous studies. In several cases we provide more accurate parameters, which was possible due to the high quality of the spectra. The most important aspect of our results is that parameters for all 23 stars were determined in a homogeneous way.

5.3 Surface gravity from pressure-sensitive lines

For cool stars there are strong pressure-sensitive lines that can be used to constrain the $\log g$ parameter. Commonly used lines are Mg Ib, Na I D, and the calcium lines at $\lambda 6122 \text{ \AA}$ and $\lambda 6262 \text{ \AA}$ (Gray 2005). We follow the approach described by Fuhrmann et al. (1997) in which the Van der Waals constants are adjusted until the $\log g$ parameter of the Sun is consistent with the canonical value, $\log g_{\odot} = \log M_{\odot}/R_{\odot}^2 = 4.437$. We used the FTS spectrum of the Sun and checked that a solar spectrum of the Sun from HARPS gave consistent results (for details see Bruntt, Fridlund & Deleuil 2010, A&A, submitted). When fitting the wide lines we first determine the abundance of the element from weaker lines. The same is true for $v \sin i$ and macroturbulence although the result is less sensitive to this.

A serious problem, especially for early-type stars is the normalization of the continuum around the Mg Ib lines around 5167, 5173 and 5184 \AA . The lines are so wide that it is difficult to normalize the spectra objectively, and two of the lines lie close and therefore have no continuum between them. We found that the continuum in the red wing (around 5160 \AA) is impossible to define for stars earlier than K0, and therefore only the 5184 \AA line can be used reliably. We only used the wings of the Na I D lines to check for consistency, since the region is affected by telluric lines. The Ca lines are not as wide as the Mg Ib lines and it is easier to define the continuum. Another advantage of the Ca lines is that there are several weak lines available, so the Ca abundance is well-determined. There are only a few weak Mg lines available, and this affects the accuracy of $\log g$ determined from the Mg Ib lines.

To fit the observed spectrum we calculated synthetic spectra for three values of $\log g$. We then calculated the χ^2 value for a few selected regions that are not seriously affected by blending lines. Bruntt, Fridlund & Deleuil (2010, A&A, submitted) gave a

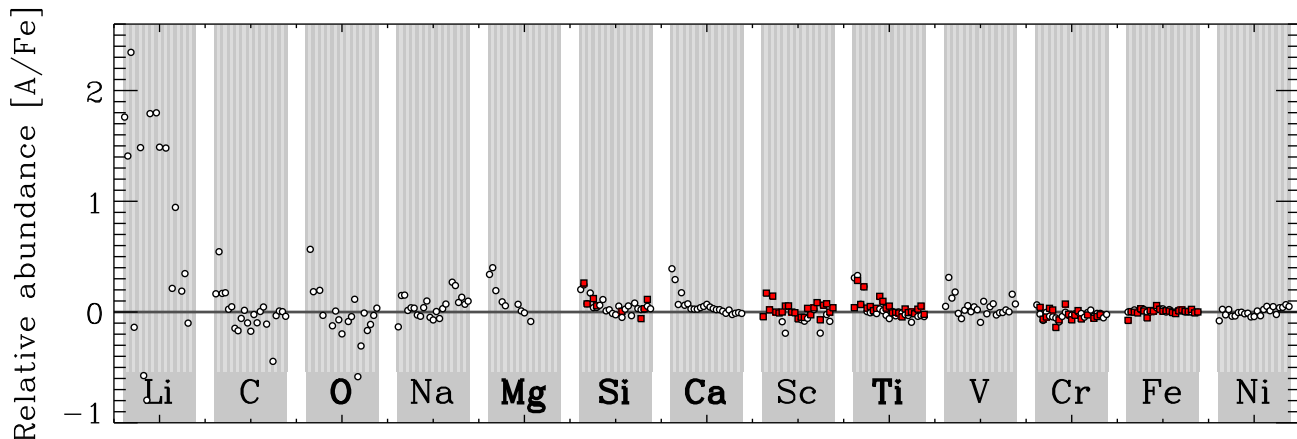


Figure 10. Mean abundances of 13 elements in 23 solar-type stars sorted by $[\text{Fe}/\text{H}]$ increasing from left to right. To be able to show the results on the same scale abundances are measured relative to Fe. The mean abundance from neutral and ionized lines are marked with circles and box symbols, respectively. The names of the α elements are written with bold font: notice the generally higher abundance for the low metallicity stars. Abundances for each individual star is given in Table 4.

more detailed description of the method when applied to α Cen B. In Table 3 we compare the $\log g$ values determined from different techniques. It is seen that the precision on the $\log g$ determination changes a lot from star to star and is due to the change in sensitivity depending on the spectral type. In general, the Ca lines at $\lambda 6122 \text{ \AA}$ and $\lambda 6262 \text{ \AA}$ are the most useful, but the Mg 1b line is applicable for the early-type stars. For the final spectroscopic value of $\log g$ we calculated the weighted mean value which is given in column 4.

In Fig. 9 (top panel) we compare the $\log g$ values determined from spectroscopy (weighted mean value using FeI+II and the Ca lines) with that from the combination of radius and mass through

$$\log g = \log M/M_{\odot} - 2 \log R/R_{\odot} + \log g_{\odot}. \quad (7)$$

Different symbols in Fig. 9 are used to indicate the source of M and R . The radius is from Sect. 4.1, as found using either interferometric measurements (filled symbols) or the combination of luminosity and effective temperature (open symbols). The mass was determined from the asteroseismic information (Sect. 2) using either the $\Delta\nu$ (circles) or ν_{max} (box symbols). There is generally good agreement, with a mean difference of $+0.061 \pm 0.077$ dex. Instead of using the intrinsic uncertainties on $\log g$ given in Table 3, we shall adopt 0.08 dex (the rms scatter) as the uncertainty on $\log g$ for all stars in the sample. This is very similar to the uncertainty adopted in other studies of large samples of stars (Valenti & Fischer 2005; Fuhrmann 2004).

Finally, we find excellent agreement (< 0.1 dex) when comparing the results in Table 3 for the four binary stars, for which absolute M and R is available (although R for 70 Oph A is not a direct measurement). This further supports that the indirect methods give consistent results for the surface gravity.

5.4 Chemical composition

With the atmospheric parameters determined from FeI+II and the pressure-sensitive lines, we computed the mean abundances for 13 elements. In Table 4 we list the mean abundances and in Fig. 10 we plot the abundances. To be able to show the results on the same scale we have offset the abundances by the mean abundance of FeI lines. It can be seen that FeI+II agree since this was a requirement when adjusting the atmospheric parameters. There is some scatter

in the light elements (Li, C, O), while most of the metals have quite low scatter. This indicates that a simple scaling from the solar abundance using just $[\text{Fe}/\text{H}]$ is a good approximation. However, for the stars with low metallicity we see a clear increase in the abundance of the α elements (Ca, Si and Ti). This α enhancement is shown in more detail for τ Cet in Fig. 7.

Holmberg et al. (2007) presented a calibration of $[\text{Fe}/\text{H}]$ based on Strömgen indices and in the last two columns in Table 2 we compare them with the spectroscopic values. The comparison is shown in Fig. 9 in the bottom panel. There is excellent agreement with a mean difference of $\Delta[\text{Fe}/\text{H}] = -0.054 \pm 0.102$ (rms scatter).

5.5 Projected rotational velocity and macroturbulence

The mean rotational velocity is important for asteroseismic modelling since the observed frequencies are split depending on the projected rotation rate. The high-precision photometry from *CoRoT* and *Kepler* provides indirect measures of the rotational period for solar-type star as spots traverse the surface. However, in the case of the solar-type *CoRoT* target HD 49385, Deheuvels et al. (A&A, 2010, accepted) could not directly measure the rotation period from the photometry. Instead they used the spectroscopically measured $v \sin i$ to rule out one of the possible scenarios when interpreting the asteroseismic data.

The shape of a spectral line depends on various physical processes on a microscopic scale (atomic absorption, pressure and thermal broadening) but also depends on the macroscopic velocity fields in the photosphere due to convection cells and the rotation of the star. For some lines the detailed line shape is further affected by hyperfine structure and the Zeeman effect in the case of strong magnetic fields.

We used isolated spectral lines to determine the projected rotational velocity ($v \sin i$) and macroturbulence of the target stars following similar assumptions and methods as Saar & Osten (1997) and Reddy et al. (2002). In our analysis we described the broadening mechanisms with some common simplifications. We included the broadening due to the projected rotational velocity ($v \sin i$) in the formulation of Gray (2005), instrumental broadening (a Gaussian profile), macroturbulence (also a Gaussian profile), and line

Table 3. Surface gravities from methods (columns 2–9). The macroturbulence, microturbulence and $v \sin i$ from the spectroscopic analysis (columns 10–12) have uncertainties of 0.6, 0.07, and 0.6 km s^{-1} .

Star	Binary $M + R$	Asteroeis. ρ, R	Mean of spec. methods	Spectroscopic methods					v_{mac} [km/s]	v_{mic} [km/s]	$v \sin i$ [km/s]
				FeI+II	Mg Ib	Ca-6122	Ca-6162	Ca-6439			
β Hya		3.955 ± 0.018	3.843 ± 0.081	3.92 ± 0.11	3.68 ± 0.32	3.72 ± 0.18	3.81 ± 0.18	3.86 ± 0.81	2.9	1.16	2.7
τ Cet		4.533 ± 0.018	4.456 ± 0.048	4.48 ± 0.10	4.91 ± 0.22	4.39 ± 0.10	4.42 ± 0.07	4.57 ± 0.24	0.9	0.72	0.7
ι Hor		4.399 ± 0.022	4.402 ± 0.063	4.41 ± 0.11	4.37 ± 0.12	4.41 ± 0.16	4.39 ± 0.13	4.70 ± 0.42	3.3	1.04	5.3
α For		4.003 ± 0.033	3.802 ± 0.077	3.82 ± 0.11	3.72 ± 0.13	3.85 ± 0.21	4.08 ± 0.34	4.22 ± 0.89	3.7	1.29	3.9
δ Eri		3.827 ± 0.018	3.773 ± 0.054	3.74 ± 0.10	3.64 ± 0.39	3.74 ± 0.11	3.85 ± 0.09	3.69 ± 0.19	0.9	0.89	0.7
α Men			4.425 ± 0.044	4.45 ± 0.10	4.43 ± 0.12	4.36 ± 0.13	4.42 ± 0.06	4.55 ± 0.25	1.0	0.93	0.6
Procyon A	3.976 ± 0.016	3.972 ± 0.018	3.891 ± 0.090	4.01 ± 0.14	3.80 ± 0.12	3.86 ± 0.75	3.90 ± 0.43	4.46 ± 0.70	4.6	1.69	2.8
171 Pup		4.244 ± 0.023	4.088 ± 0.074	4.17 ± 0.10	3.98 ± 0.12	4.37 ± 0.58	4.03 ± 0.32	4.26 ± 0.89	1.9	1.21	1.6
ξ Hya		2.883 ± 0.032	2.809 ± 0.077	2.76 ± 0.10	2.37 ± 0.42	2.85 ± 0.18	3.10 ± 0.20	2.65 ± 0.39	3.8	1.20	2.4
β Vir		4.125 ± 0.018	3.983 ± 0.068	4.01 ± 0.11	4.01 ± 0.16	3.91 ± 0.12	4.06 ± 0.21	4.04 ± 0.54	3.6	1.29	2.0
η Boo		3.822 ± 0.019	3.899 ± 0.052	3.88 ± 0.11	3.87 ± 0.06	4.07 ± 0.27	4.08 ± 0.19	4.20 ± 0.49	5.3	1.74	11.9
α Cen A	4.307 ± 0.005	4.318 ± 0.017	4.309 ± 0.055	4.28 ± 0.10	4.32 ± 0.11	4.28 ± 0.21	4.32 ± 0.09	4.60 ± 0.43	2.3	1.00	1.9
α Cen B	4.538 ± 0.008	4.530 ± 0.018	4.515 ± 0.036	4.45 ± 0.10	4.01 ± 0.50	4.53 ± 0.07	4.51 ± 0.05	4.65 ± 0.16	0.8	0.83	1.0
HR 5803		4.229 ± 0.023	4.083 ± 0.077	4.05 ± 0.14	4.02 ± 0.14	4.15 ± 0.13	4.17 ± 0.28	4.22 ± 0.89	4.1	1.31	5.2
γ Ser		4.169 ± 0.032	4.009 ± 0.076	4.01 ± 0.11	3.93 ± 0.11	4.33 ± 0.46	4.48 ± 0.32	5.33 ± 1.17	3.9	1.29	10.2
μ Ara		4.228 ± 0.023	4.136 ± 0.060	4.25 ± 0.10	4.04 ± 0.16	3.92 ± 0.20	4.12 ± 0.10	4.03 ± 0.39	2.6	1.05	1.4
70 Oph A	4.468 ± 0.030	4.555 ± 0.023	4.569 ± 0.028	4.59 ± 0.10	4.50 ± 0.23	4.53 ± 0.06	4.57 ± 0.04	4.73 ± 0.15	1.5	0.93	0.9
η Ser		3.029 ± 0.037	2.955 ± 0.072	2.96 ± 0.10	2.90 ± 0.25	2.88 ± 0.25	2.98 ± 0.13	3.03 ± 0.55	2.1	1.04	1.1
β Aql		3.525 ± 0.036	3.550 ± 0.083	3.49 ± 0.10	3.49 ± 0.33	3.67 ± 0.37	3.76 ± 0.19	3.65 ± 0.52	2.1	0.88	0.9
δ Pav		4.306 ± 0.034	4.319 ± 0.054	4.30 ± 0.10	4.43 ± 0.26	4.16 ± 0.15	4.34 ± 0.08	4.48 ± 0.22	1.7	0.95	1.0
γ Pav		4.397 ± 0.022	4.195 ± 0.079	4.24 ± 0.11	4.06 ± 0.14	4.33 ± 0.27	4.26 ± 0.24	4.39 ± 1.48	2.0	1.19	1.8
τ PsA		4.240 ± 0.021	4.096 ± 0.073	4.09 ± 0.14	4.05 ± 0.10	4.27 ± 0.25	4.24 ± 0.26	5.08 ± 0.71	4.1	1.30	13.6
ν Ind		3.432 ± 0.035	3.526 ± 0.090	3.48 ± 0.10	4.50 ± 0.38	3.38 ± 0.28	3.49 ± 0.47	2.84 ± 1.19	1.4	1.35	1.1

broadening parameters from the VALD database. In addition, when calculating the synthetic profiles we introduced the microturbulence parameter. We note that from bisector analysis of the asymmetry of spectral lines much more can be learned about the granulation. This requires individual spectra with very high resolution and is beyond the scope of the current work (Dravins 2008; Allende Prieto et al. 2002).

Since we have used different spectrographs, we made careful estimations of the instrumental profiles. This was done by measuring the widths of several telluric lines from 6279–6304 Å. Up to 19 (typically 12–15) lines could be used depending on how the telluric lines were shifted and blended with the stellar lines. The telluric lines were fitted with Gaussian profiles and the instrumental resolution was estimated from the mean FWHM ($\Delta\lambda$) of these profiles, i.e. $R = \langle \lambda / \Delta\lambda \rangle$. In general we measured a resolution 10–15% lower than the nominal values found in the instrument descriptions. We have assumed that the telluric lines have zero width, but in fact telluric lines have non-zero widths that change with observing conditions and airmass. Thus, our assumption will indeed give a tendency to underestimate the resolution of the spectrograph. For the HARPS spectra we also measured R from the Th-Ar calibration spectra, and in this case we measured $R = 107\,000 \pm 3000$ (rms scatter from eight lines), which is close to the instrumental specification ($R = 115\,000$, Mayor et al. 2003).

To select the most suitable lines for the determination of $v \sin i$ we chose lines from the abundance analysis that are present in at least 60% of all stars. All lines are relatively weak, with equivalent widths in the Solar spectrum between 20 and 100 mÅ. For each line we fixed the fitted values of the abundance and the instrumental resolution. We then convolved the synthetic line by different combinations of $v \sin i$ and macroturbulence in a regular grid with

steps of 0.15 km s^{-1} . We calculated the χ^2 value of each fit from the sum over a region around each line⁵:

$$\chi^2 = \frac{1}{n} \sum_{i=1}^N \frac{(O_i - S_i)^2}{\sigma^2}, \quad (8)$$

where N is the total number of observed data points and n is the number of degrees of freedom in the fit: $n = N - 3$, since three parameters are being fitted: wavelength shift, $v \sin i$ and macroturbulence. O_i and S_i denote the relative flux of the observed and synthetic profile and σ is the measured noise in the continuum (see Reddy et al. 2002). Typically 10–30 lines are used for each star. The final values of $v \sin i$ and macroturbulence are calculated as the mean value and the rms value is taken as the $1-\sigma$ uncertainty.

In the bottom panel in Fig. 11 we show the $v \sin i$ values of the target stars, showing that there are more fast rotators among the early type stars. We have compared the determined $v \sin i$ and macroturbulence with similar studies in the literature in Table B1 in Appendix B. We find a good agreement with Saar & Osten (1997) for four stars. We have six stars in common with Valenti & Fischer (2005), but they did not include macroturbulence in their description of the broadening. We find that by quadratically adding our values for $v \sin i$ and macroturbulence we get good agreement with the $v \sin i$ values from Valenti & Fischer (2005). Dravins et al. (1993) and Allende Prieto et al. (2002) used high-resolution spectra of β Hya and Procyon A. They used 3D time-dependent atmosphere models but we still get almost perfect agreement with these two studies for $v \sin i$.

⁵ The range is typically ± 0.2 to $\pm 0.5 \text{ Å}$ for $v \sin i$ values from 1 to 15 km s^{-1} .

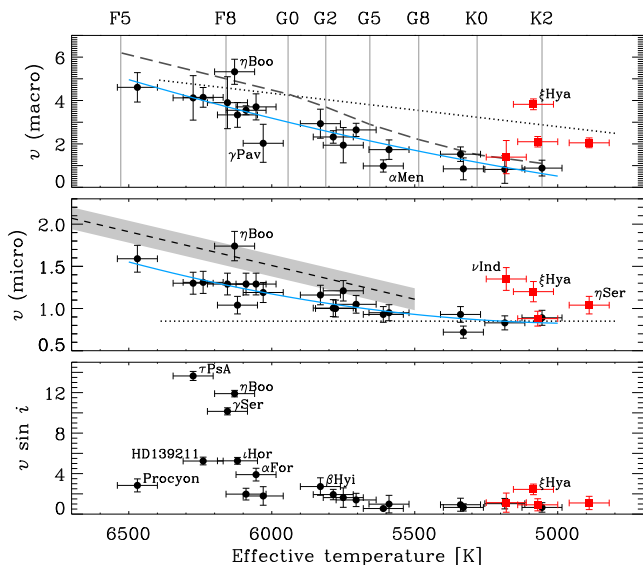


Figure 11. Macro- and microturbulence and $v \sin i$ determined from the spectroscopic analysis. In the two top panels the solid line is a second order fit to the data (Eqs. 9 and 10). In the top panel the dashed line is adopted from Gray (2005) and in the middle panel the dashed line and shaded region is the calibration of microturbulence from Edvardsson et al. (1993). The dotted lines are the results from Valenti & Fischer (2005) (see discussion in the text).

5.6 Calibrations of macro- and microturbulence

In Fig. 11 we show the determined values of v_{macro} and v_{micro} (also given in Table 3). In the top panel we have marked the approximate spectral type following the tabulation by Gray (2005). The solid lines are polynomial fits to the data while discarding the four giant stars and two apparent outliers (η Boo and α Men). The fits are expressed as a function of T_{eff} :

$$v_{\text{macro}} = 2.26 + 2.90 \cdot 10^{-3} \Delta T + 5.86 \cdot 10^{-7} \Delta T^2 \text{ km s}^{-1} \quad (9)$$

$$v_{\text{micro}} = 1.01 + 4.56 \cdot 10^{-4} \Delta T + 2.75 \cdot 10^{-7} \Delta T^2 \text{ km s}^{-1}, \quad (10)$$

where $\Delta T = T_{\text{eff}}^* - 5700 \text{ K}$; T_{eff}^* is the spectroscopic value. These calibrations are valid for unevolved stars ($\log g > 4.0$) in the range 5000–6500 K and the rms scatter for the fits are 0.27 and 0.09 km s^{-1} , respectively.

The dashed line in the top panel in Fig. 11 is from Gray (2005) (see his Fig. 17.10 for luminosity class V) and the dotted line is the upper limit on macroturbulence from Valenti & Fischer (2005). We find a systematically lower v_{macro} for all stars. However, the source of the data in Gray (2005) is not known, so we cannot identify the reason for the apparent discrepancy. To determine upper limits on macroturbulence, Valenti & Fischer (2005) assumed $v \sin i = 0 \text{ km s}^{-1}$, so it is not surprising that we find lower values for all spectral types. In the middle panel of Fig. 11 we compare our v_{micro} values with the calibration of Edvardsson et al. (1993), valid in the range from 5500–6800 K: $v_{\text{micro}} = 1.25 + 8 \times 10^{-4} (T_{\text{eff}} - 6000) - 1.30 (\log g - 4.5)$. The dashed line corresponds to $\log g = 4.3$ and the gray shaded area marks the range for changes in $\log g$ of ± 0.1 dex. Edvardsson et al. (1993) report that the scatter of individual stars is 0.3 km s^{-1} around this relation. They used only a very limited number lines of Fe I and Ni I (up to 17) to constrain v_{micro} , while we have used hundreds of lines in each star. However, the larger sample of Edvardsson et al. (1993) (157 stars) allowed

them to include the variation with $\log g$. Our v_{micro} calibration predicts values that are typically 0.3 km s^{-1} lower. Edvardsson et al. (1993) used $v_{\text{micro}} = 1.15 \text{ km s}^{-1}$ whereas we find 0.95 km s^{-1} for the Solar spectrum. Valenti & Fischer (2005) studied a large sample of over 1000 stars by making a “global fit” to the observed spectra. They found no dependence of microturbulence and T_{eff} and adopted a fixed value of 0.85 km s^{-1} , indicated by the dotted horizontal line in the middle panel in Fig. 11. By studying saturated line profiles, Landstreet et al. (2009) demonstrated that higher convective velocity implies a higher microturbulence in A and F type stars. It is important to note that microturbulence is a fitting parameter that is only conceptually linked to convective motion on small scales (see discussions in Valenti & Fischer 2005, Gray 2005, and Dravins & Nordlund 1990). It is therefore difficult to compare v_{micro} for different analysis methodologies and different model atmospheres.

6 CONCLUSIONS AND FUTURE OUTLOOK

We have determined the fundamental parameters of 23 bright solar-type stars: mass, radius, and luminosity. Our goal was to assess the absolute accuracy of indirect techniques by comparing our results with direct techniques that are only weakly model-dependent. The adopted direct techniques used interferometric data, bolometric fluxes and parallaxes, or orbits of binary stars, and could be applied to 10 of the stars in the sample. The indirect methods used asteroseismic data, spectroscopic data, and Strömgren photometry. We also presented a detailed spectroscopic analysis of high-quality spectra. This included the determination of T_{eff} , chemical composition, surface gravity, and projected rotational velocity. We compared the determined parameters with results from the literature that use similar spectroscopic methods, and found good agreement except for a few cases. In summary, indirect mass and radius estimates give good results, with some evidence for systematic errors in the luminosity of cool stars, while spectroscopic T_{eff} values need a slight adjustment. For future analyses, we conclude that from spectroscopic analysis of a high-quality spectrum, T_{eff} can be determined to 80 K, $\log g$ to 0.08 dex, and $[\text{Fe}/\text{H}]$ to 0.07 dex. Similar conclusions, based on larger spectroscopic data sets, were reached by Fuhrmann (2004) and Valenti & Fischer (2005).

We have determined a homogeneous set of parameters for 23 solar-type stars that will be valuable for future asteroseismic campaigns. Observations have already been carried out on 22 of the 23 stars and have shown that the stars are indeed oscillating. In the near future several of the stars analysed here will be targets for the Stellar Observations Network Group (SONG; Grundahl et al. 2008, 2009). Such lists of bright targets for asteroseismology have previously been given by Bedding et al. (1996) and Pijpers (2003). Although these are extremely useful for selecting targets, they may be of limited use when doing detailed asteroseismic analyses. For example, the Bedding et al. (1996) study pre-dates the *Hipparcos* catalogue, while the parameters tabulated by Pijpers (2003) were determined from multiple studies using different methods and varying quality of observations, e.g. 18 different papers cited for the effective temperature of 40 stars.

Looking ahead, improvements in f_{bol} determinations may soon be possible. The accuracy is limited by the accuracy of the stellar flux scale, which is currently based on the Hayes & Latham (1975) absolute flux measurements of Vega. This gives a minimum uncertainty of around 2% on f_{bol} . The internal uncertainties in spectrophotometry of the individual stars contribute at least 1% to

Table 4. Abundances and number of lines used in spectral analysis of 23 target stars, sorted by metallicity. The uncertainty on the abundances is 0.07 dex. The data are shown graphically in Fig. 10.

	ν Ind	171 Pup	γ Pav	τ Cet	α For	γ Ser	β Aql	η Ser	β Hyi	Procyon A	HR 5803	τ PsA	
Li I	+0.21	1 +0.56	1 +1.61	1 -0.61	1	+1.22	1 -0.73	1 -0.91	1 +1.68	1	+1.74	1 +1.50	1
C I	-1.39	2 -0.31	2 -0.57	2 -0.30	1 -0.28	4 -0.22	4 -0.30	1 -0.29	1 -0.16	1 -0.04	4 -0.15	5 -0.17	3
O I		-0.29	2 -0.55	3	-0.11	2 -0.29	2		-0.23	2 -0.04	4 -0.13	2 -0.19	2
Na I	-1.69	1 -0.70	3 -0.60	5 -0.46	3 -0.27	2 -0.23	3 -0.18	2 -0.16	2 -0.07	1 +0.03	4 -0.10	3 -0.06	2
Mg I	-1.21	1 -0.45	2 -0.54	2	-0.21	2 -0.21	2			+0.02	2 -0.05	2 -0.00	2
Si I	-1.35	1 -0.61	18 -0.66	14 -0.30	24 -0.27	24 -0.22	16 -0.09	22 -0.01	23 -0.10	22 -0.03	28 -0.07	26 -0.02	17
Si II		-0.59	1 -0.66	1	-0.18	1 -0.21	1						
Ca I	-1.16	4 -0.56	13 -0.66	19 -0.30	8 -0.24	13 -0.19	9 -0.12	5 -0.09	6 -0.05	5 -0.01	18 -0.00	11 +0.08	7
Sc I							-0.24	1 -0.31	1				
Sc II	-1.60	2 -0.68	6 -0.73	6 -0.33	6 -0.31	4 -0.27	5 -0.15	7 -0.07	6 -0.05	5 -0.04	8 -0.06	6 -0.05	5
Ti I	-1.25	3 -0.52	24 -0.67	26 -0.25	28 -0.30	22 -0.27	14 -0.15	17 -0.13	15 -0.08	8 -0.04	27 -0.09	20 -0.05	4
Ti II	-1.51	1 -0.58	9 -0.68	12 -0.27	11 -0.28	8 -0.27	9 -0.19	8 -0.10	4 +0.03	1 +0.02	17 -0.04	5 +0.06	3
V I	-1.50	7 -0.54	8 -0.61	3 -0.30	10 -0.32	7 -0.32	4 -0.14	8 -0.06	11 -0.10	7 -0.01	6 -0.03	8 -0.09	6
Cr I	-1.49	2 -0.87	11 -0.81	13 -0.48	18 -0.34	19 -0.31	14 -0.21	12 -0.21	10 -0.15	2 -0.05	22 -0.09	13 -0.02	12
Cr II		-0.81	4 -0.80	4 -0.52	3 -0.27	3 -0.25	4 -0.29	3 -0.19	2	+0.02	5 -0.08	2 -0.06	2
Fe I	-1.55	187 -0.85	183 -0.74	219 -0.48	202 -0.31	213 -0.27	178 -0.15	179 -0.12	168 -0.11	92 -0.05	260 -0.06	216 +0.01	169
Fe II	-1.63	17 -0.86	22 -0.74	22 -0.48	16 -0.28	24 -0.26	16 -0.21	17 -0.11	13 -0.10	9 +0.01	20 -0.04	16 +0.01	17
Ni I	-1.63	17 -0.83	43 -0.76	48 -0.46	54 -0.34	53 -0.30	37 -0.16	53 -0.12	46 -0.12	32 -0.06	71 -0.10	53 -0.03	35
	70 Oph A	ι Hor	α Men	δ Eri	β Vir	η Boo	ξ Hya	α Cen A	μ Ara	α Cen B	δ Pav		
Li I		+1.62	1	+0.37	1 +1.06	1	+0.39	1 +0.57	1 +0.19	1			
C I	+0.09	2 +0.04	3 +0.16	4 +0.21	1 +0.01	4	-0.24	1 +0.19	3 +0.30	4 +0.32	1 +0.34	3	
O I		+0.06	2 +0.11	2 +0.28	1 -0.47	3 -0.08	3 +0.19	2 +0.05	4 +0.18	2 +0.28	1 +0.42	3	
Na I	+0.11	2 +0.08	1 +0.18	2 +0.23	1 +0.10	1 +0.50	1 +0.44	1 +0.31	2 +0.43	2 +0.38	1 +0.48	1	
Mg I		+0.06	2										
Si I	+0.16	17 +0.09	26 +0.18	19 +0.22	12 +0.08	5 +0.31	10 +0.23	11 +0.24	22 +0.32	23 +0.36	12 +0.41	14	
Si II		+0.15	1					+0.16	1 +0.32	1 +0.43	1		
Ca I	+0.15	2 +0.17	10 +0.17	5 +0.18	1 +0.12	10 +0.21	2 +0.22	1 +0.20	5 +0.28	5 +0.31	2 +0.37	4	
Sc I	+0.04	1 +0.06	1 +0.10	1	+0.14	1	+0.01	1	+0.27	1 +0.23	1		
Sc II	+0.06	8 +0.09	4 +0.19	7 +0.14	2 +0.15	4 +0.31	3 +0.13	1 +0.28	4 +0.37	5 +0.31	6 +0.42	5	
Ti I	+0.11	36 +0.11	24 +0.15	20 +0.15	25 +0.09	27 +0.19	3 +0.11	20 +0.21	22 +0.26	25 +0.28	16 +0.34	13	
Ti II	+0.10	10 +0.13	10 +0.15	11 +0.12	1 +0.12	13 +0.22	1 +0.20	4 +0.21	7 +0.30	9 +0.37	1 +0.28	3	
V I	+0.20	17 +0.13	9 +0.20	5 +0.24	7 +0.09	1 +0.22	7 +0.20	9 +0.24	10 +0.30	9 +0.47	16 +0.45	10	
Cr I	+0.09	13 +0.14	14 +0.14	12 +0.11	7 +0.11	17 +0.24	4 +0.16	7 +0.21	11 +0.28	11 +0.26	12 +0.36	8	
Cr II	+0.08	4 +0.15	1 +0.09	4	+0.09	5	+0.14	1 +0.18	2 +0.27	5			
Fe I	+0.11	217 +0.14	206 +0.15	166 +0.16	116 +0.11	188 +0.23	70 +0.20	99 +0.22	184 +0.29	186 +0.31	129 +0.38	126	
Fe II	+0.12	13 +0.15	20 +0.15	21 +0.15	7 +0.12	18 +0.24	8 +0.21	10 +0.22	19 +0.32	16 +0.30	8 +0.38	12	
Ni I	+0.12	61 +0.11	58 +0.18	55 +0.21	32 +0.13	62 +0.27	22 +0.18	24 +0.26	60 +0.34	56 +0.38	33 +0.43	34	

the final error determination. This limits direct T_{eff} determinations to no better than around ± 50 K for solar-type stars. The ACCESS project (Absolute Color Calibration Experiment for Standard Stars; Kaiser et al. 2008) should determine the absolute flux scale to better than 1%. This, together with improved stellar spectrophotometry (Adelman et al. 2007), will enable f_{bol} (and hence T_{eff}) to be determined to higher accuracy.

As a future outlook on the subject of accurate stellar parameters, we note that while interferometric measurements are available for only ten of the stars in our sample, all of the targets should now be possible to observe with the recent improvements in instrumentation like the PAVO instrument at CHARA and SUSI (Ireland et al. 2008) or AMBER at VLTI (Petrov et al. 2007). We strongly encourage such measurements to improve the calibration of secondary methods to characterize solar-type stars. This will be invaluable to improve the modelling efforts using asteroseismology of more distant targets of the *CoRoT* and *Kepler* missions.

ACKNOWLEDGMENTS

This project was supported by the Australian and Danish Research Councils. We made use of the SIMBAD database, operated at CDS, Strasbourg, France. This research has made use of NASA's Astrophysics Data System Bibliographic Services. We used spectra from HARPS obtained from the ESO archive under programme IDs 60.A-9036, 073.D-0590, 073.D-0578, 073.D-0590, 074.D-0380, 075.D-0760, 076.D-0103, 077.D-0498, 077.C-0530, 077.D-0720, 078.D-0067, 078.D-0492, 078.C-0233, 079.D-0466, 079.C-0681, 080.C-0712, and 081.D-0531.

REFERENCES

- Adelman S. J., Gulliver A. F., Smalley B., Pazder J. S., Younger P. F., Boyd L. J., Epan D., Younger T., 2007, in C. Sterken ed., *The Future of Photometric, Spectrophotometric and Polarimetric Standardization* Vol. 364 of *Astronomical Society of the Pacific Conference Series*, *The ASTRA Spectrophotometer: Design and Overview*. p. 255

- Aerts C., Christensen-Dalsgaard J., Cunha M., Kurtz D. W., 2008, *Sol. Phys.*, 251, 3
- Alekseeva G. A., Arkharov A. A., Galkin V. D., Hagen-Thorn E. I., Nikanorova I. N., Novikov V. V., Novopashenny V. B., Pakhomov V. P., Ruban E. V., Shchegolev D. E., 1996, *Baltic Astronomy*, 5, 603
- Allende Prieto C., Asplund M., López R. J. G., Lambert D. L., 2002, *ApJ*, 567, 544
- Ammler-von Eiff M., Santos N. C., Sousa S. G., Fernandes J., Guillot T., Israelian G., Mayor M., Melo C., 2009, *A&A*, 507, 523
- Arentoft T., Kjeldsen H., Bedding T. R., Bazot M., Christensen-Dalsgaard J., Dall T. H., Karoff C., Carrier F., Eggenberger P., Sosnowska D., Wittenmyer R. A., Endl M., Metcalfe 2008, *ApJ*, 687, 1180
- Asplund M., 2005, *ARA&A*, 43, 481
- Aufdenberg J. P., Ludwig H., Kervella P., 2005, *ApJ*, 633, 424
- Barban C., de Ridder J., Mazumdar A., Carrier F., Eggenberger P., de Ruyter S., Vanautgaerden J., Bouchy F., Aerts C., 2004, in Danesy D., ed., *SOHO 14 Helio- and Asteroseismology: Towards a Golden Future Vol. 559 of ESA Special Publication. Detection of Solar-Like Oscillations in Two Red Giant Stars*. p. 113
- Basu S., Chaplin W. J., Elsworth Y., 2010, *ApJ*, 710, 1596
- Bedding T. R., Butler R. P., Carrier F., Bouchy F., Brewer B. J., Eggenberger P., Grundahl F., Kjeldsen H., McCarthy C., Nielsen T. B., Retter A., Tinney C. G., 2006, *ApJ*, 647, 558
- Bedding T. R., Kjeldsen H., 2008, in van Belle G., ed., *14th Cambridge Workshop on Cool Stars, Stellar Systems, and the Sun Vol. 384 of Astronomical Society of the Pacific Conference Series, Asteroseismology from Solar-Like Oscillations*. p. 21
- Bedding T. R., Kjeldsen H., Reetz J., Barbey B., 1996, *MNRAS*, 280, 1155
- Bessell M. S., Castelli F., Plez B., 1998, *A&A*, 333, 231
- Bigot L., Kervella P., Thévenin F., Ségransan D., 2006, *A&A*, 446, 635
- Bouchy F., Bazot M., Santos N. C., Vauclair S., Sosnowska D., 2005, *A&A*, 440, 609
- Bouchy F., Carrier F., 2003, *Ap&SS*, 284, 21
- Breger M., 1976, *ApJS*, 32, 7
- Bruntt H., 2009, *A&A*, 506, 235
- Bruntt H., Bikmaev I. F., Catala C., Solano E., Gillon M., Magain P., Van't Veer-Menneret C., Stütz C., Weiss W. W., Ballereau D., Bouret J. C., Charpinet S., Hua T., Katz D., Lignières F., Lueftinger T., 2004, *A&A*, 425, 683
- Bruntt H., De Cat P., Aerts C., 2008, *A&A*, 478, 487
- Caffau E., Ludwig H., Steffen M., Ayres T. R., Bonifacio P., Cayrel R., Freytag B., Plez B., 2008, *A&A*, 488, 1031
- Carrier F., Eggenberger P., 2006, *A&A*, 450, 695
- Carrier F., Eggenberger P., D'Alessandro A., Weber L., 2005, *New Astronomy*, 10, 315
- Chaplin W. J., Appourchaux T., Elsworth Y., Garcia R. A., Houdek G., Karoff C., Metcalfe T. S., Molenda-Zakowicz J., Monteiro M. J. P. F. G., Thompson M. J., Brown T. M., Christensen-Dalsgaard J., Gilliland R. L., 2010, *ArXiv e-prints* 1001.0506
- Christensen-Dalsgaard J., 2008, *Ap&SS*, 316, 13
- Christensen-Dalsgaard J., Kjeldsen H., Brown T. M., Gilliland R. L., Arentoft T., Frandsen S., Quirion P.-O., Borucki W. J., Koch D., Jenkins J. M., 2010, *ApJ*, accepted
- Cox A. N., 2000, *Allen's Astrophysical Quantities*. New York: AIP Press; Springer, 2000
- di Folco E., Absil O., Augereau J.-C., Mérand A., Coudé Du Foresto V., Thévenin F., Defrère D., Kervella P., Ten Brummelaar T. A., McAlister H. A., Ridgway S. T., Sturmman J., Sturmman L., Turner N. H., 2007, *A&A*, 475, 243
- Dravins D., 2008, *A&A*, 492, 199
- Dravins D., Lindegren L., Nordlund A., Vandenberg D. A., 1993, *ApJ*, 403, 385
- Dravins D., Nordlund A., 1990, *A&A*, 228, 184
- Edvardsson B., Andersen J., Gustafsson B., Lambert D. L., Nissen P. E., Tomkin J., 1993, *A&A*, 275, 101
- Eggenberger P., Miglio A., Carrier F., Fernandes J., Santos N. C., 2008, *A&A*, 482, 631
- Engels D., Sherwood W. A., Wamsteker W., Schultz G. V., 1981, *A&AS*, 45, 5
- Flower P. J., 1996, *ApJ*, 469, 355
- Frandsen S., Carrier F., Aerts C., Stello D., Maas T., Burnet M., Bruntt H., Teixeira T. C., de Medeiros J. R., Bouchy F., Kjeldsen H., Pijpers F., Christensen-Dalsgaard J., 2002, *A&A*, 394, L5
- Fuhrmann K., 1998, *A&A*, 338, 161
- Fuhrmann K., 2004, *Astronomische Nachrichten*, 325, 3
- Fuhrmann K., 2008, *MNRAS*, 384, 173
- Fuhrmann K., Pfeiffer M., Frank C., Reetz J., Gehren T., 1997, *A&A*, 323, 909
- Gatewood G., Han I., 2006, *AJ*, 131, 1015
- Ghezzi L., Cunha K., Smith V. V., Margheim S., Schuler S., de Araújo F. X., de la Reza R., 2009, *ApJ*, 698, 451
- Girard T. M., Wu H., Lee J. T., Dyson S. E., van Altena W. F., Horch E. P., Gilliland R. L., Schaefer K. G., Bond H. E., Ftacclas C., Brown R. H., Toomey D. W., Shipman H. L., Provencal J. L., Pourbaix D., 2000, *AJ*, 119, 2428
- Girardi L., Bertelli G., Bressan A., Chiosi C., Groenewegen M. A. T., Marigo P., Salasnich B., Weiss A., 2002, *A&A*, 391, 195
- Gray D. F., 2005, *The Observation and Analysis of Stellar Photospheres*. Cambridge University Press (UK) 2005
- Grevesse N., Asplund M., Sauval A. J., 2007, *Space Sci. Reviews*, 130, 105
- Grundahl F., Arentoft T., Christensen-Dalsgaard J., Frandsen S., Kjeldsen H., Rasmussen P. K., 2008, *Journal of Physics Conference Series*, 118, 012041
- Grundahl F., Christensen-Dalsgaard J., Kjeldsen H., Jørgensen U. G., Arentoft T., Frandsen S., Kjærgaard P., 2009, *ArXiv e-prints* 0908.0436
- Guenther D. B., Kallinger T., Reegen P., Weiss W. W., Matthews J. M., Kuschnig R., Marchenko S., Moffat A. F. J., Rucinski S. M., Sasselov D., Walker G. A. H., 2005, *ApJ*, 635, 547
- Gustafsson B., Edvardsson B., Eriksson K., Jørgensen U. G., Nordlund Å., Plez B., 2008, *A&A*, 486, 951
- Hayes D. S., Latham D. W., 1975, *ApJ*, 197, 593
- Hinkle K., Wallace L., Valenti J., Harmer D., 2000, *Visible and Near Infrared Atlas of the Arcturus Spectrum 3727-9300 Å*. San Francisco: ASP
- Holmberg J., Nordström B., Andersen J., 2007, *A&A*, 475, 519
- Holmberg J., Nordström B., Andersen J., 2009, *A&A*, 501, 941
- Ireland M. J., Mérand A., ten Brummelaar T. A., Tuthill P. G., Schaefer G. H., Turner N. H., Sturmman J., Sturmman L., McAlister H. A., 2008, in *SPIE Conference Series Vol. 7013, Sensitive visible interferometry with PAVO*
- Kaiser M. E., Kruk J. W., McCandliss S. R., Sahnou D. J., Rauscher B. J., Benford D. J., Bohlin R. C., Deustua S. E., Dixon W. V., Feldman P. D., Gardner J. P., Kimble R. A., Kurucz R., Lampton M., Moos H. W., Perlmutter S., Riess A. G., Woodgate B. E., Wright E. L., 2008, in *Society of Photo-Optical Instrumen-*

- tation Engineers (SPIE) Conference Series Vol. 7014, ACCESS: absolute color calibration experiment for standard stars
- Kervella P., Thévenin F., Morel P., Berthomieu G., Bordé P., Provost J., 2004, *A&A*, 413, 251
- Kervella P., Thévenin F., Ségransan D., Berthomieu G., Lopez B., Morel P., Provost J., 2003, *A&A*, 404, 1087
- Kiehling R., 1987, *A&AS*, 69, 465
- Kjeldsen H., Bedding T. R., 1995, *A&A*, 293, 87
- Kjeldsen H., Bedding T. R., Arentoft T., Butler R. P., Dall T. H., Karoff C., Kiss L. L., Tinney C. G., Chaplin W. J., 2008, *ApJ*, 682, 1370
- Kjeldsen H., Bedding T. R., Christensen-Dalsgaard J., 2008, *ApJ*, 683, L175
- Kjeldsen H., Bedding T. R., Christensen-Dalsgaard J., 2009, in *IAU Symposium Vol. 253 of IAU Symposium, Measurements of Stellar Properties through Asteroseismology: A Tool for Planet Transit Studies*. pp 309–317
- Kupka F., Piskunov N., Ryabchikova T. A., Stempels H. C., Weiss W. W., 1999, *A&AS*, 138, 119
- Kurucz R. L., Furenlid I., Brault J., Testerman L., 1984, *Solar flux atlas from 296 to 1300 nm*. National Solar Observatory, Sunspot, New Mexico, USA
- Landstreet J. D., Kupka F., Ford H. A., Officer T., Sigut T. A. A., Silaj J., Strasser S., Townshend A., 2009, *A&A*, 503, 973
- Mayor M., Pepe F., Queloz D., Bouchy F., Rupprecht G., Lo Curto G., Avila G., Benz W., Bertaux J.-L., Bonfils X., dall T., Dekker H., Delabre B., Eckert W., Fleury M., Gilliotte A., 2003, *The Messenger*, 114, 20
- Morel M., Magnenat P., 1978, *A&AS*, 34, 477
- Mosser B., Deheuvels S., Michel E., Thévenin F., Dupret M. A., Samadi R., Barban C., Goupil M. J., 2008, *A&A*, 488, 635
- Mozurkewich D., Armstrong J. T., Hindsley R. B., Quirrenbach A., Hummel C. A., Hutter D. J., Johnston K. J., Hajian A. R., Elias II N. M., Buscher D. F., Simon R. S., 2003, *AJ*, 126, 2502
- Mozurkewich D., Johnston K. J., Simon R. S., Bowers P. F., Gaume R., Hutter D. J., Colavita M. M., Shao M., Pan X. P., 1991, *AJ*, 101, 2207
- Neuforge-Verheecke C., Magain P., 1997, *A&A*, 328, 261
- Nordgren T. E., Germain M. E., Benson J. A., Mozurkewich D., Sudol J. J., Elias II N. M., Hajian A. R., White N. M., Hutter D. J., Johnston K. J., Gauss F. S., Armstrong J. T., Pauls T. A., Rickard L. J., 1999, *AJ*, 118, 3032
- Nordgren T. E., Sudol J. J., Mozurkewich D., 2001, *AJ*, 122, 2707
- North J. R., Davis J., Bedding T. R., Ireland M. J., Jacob A. P., O’Byrne J., Owens S. M., Robertson J. G., Tango W. J., Tuthill P. G., 2007, *MNRAS*, 380, L80
- North J. R., Davis J., Robertson J. G., Bedding T. R., Bruntt H., Ireland M. J., Jacob A. P., Lacour S., O’Byrne J. W., Owens S. M., Stello D., Tango W. J., Tuthill P. G., 2009, *MNRAS*, 393, 245
- Olsen E. H., 1994, *A&AS*, 104, 429
- Perryman M. A. C., Lindegren L., Kovalevsky J., Hoeg E., Bastian U., Bernacca P. L., Crézé M., Donati F., Grenon M., van Leeuwen F., van der Marel H., 1997, *A&A*, 323, L49
- Petrov R. G., Malbet F., Weigelt G., Antonelli P., Beckmann U., Bresson Y., Chelli A., Dugué M., Duvert G., Gennari S., Glück L., Kern P., Lagarde S., Le Coarer E., Lisi F., Millour F., 2007, *A&A*, 464, 1
- Pijpers F. P., 2003, *A&A*, 400, 241
- Porto de Mello G. F., Lyra W., Keller G. R., 2008, *A&A*, 488, 653
- Pourbaix D., Nidever D., McCarthy C., Butler R. P., Tinney C. G., Marcy G. W., Jones H. R. A., Penny A. J., Carter B. D., Bouchy F., Pepe F., Hearnshaw J. B., Skuljan J., Ramm D., Kent D., 2002, *A&A*, 386, 280
- Reddy B. E., Lambert D. L., Laws C., Gonzalez G., Covey K., 2002, *MNRAS*, 335, 1005
- Reiners A., Schmitt J. H. M. M., 2003, *A&A*, 398, 647
- Saar S. H., Osten R. A., 1997, *MNRAS*, 284, 803
- Santos N. C., Israelian G., Mayor M., 2004, *A&A*, 415, 1153
- Santos N. C., Israelian G., Mayor M., Bento J. P., Almeida P. C., Sousa S. G., Ecuivillon A., 2005, *A&A*, 437, 1127
- Smith B. J., Price S. D., Baker R. I., 2004, *ApJS*, 154, 673
- Söderhjelm S., 1999, *A&A*, 341, 121
- Soubiran C., Katz D., Cayrel R., 1998, *A&AS*, 133, 221
- Sousa S. G., Santos N. C., Mayor M., Udry S., Casagrande L., Israelian G., Pepe F., Queloz D., Monteiro M. J. P. F. G., 2008, *A&A*, 487, 373
- Stello D., Chaplin W. J., Basu S., Elsworth Y., Bedding T. R., 2009, *MNRAS*, 400, L80
- Stello D., Chaplin W. J., Bruntt H., Creevey O. L., García-Hernández A., Monteiro M. J. P. F. G., Moya A., Quirion P.-O., Sousa S. G., Suárez J.-C., 2009, *ApJ*, 700, 1589
- Teixeira T. C., Kjeldsen H., Bedding T. R., Bouchy F., Christensen-Dalsgaard J., Cunha M. S., Dall T., Frandsen S., Karoff C., Monteiro M. J. P. F. G., Pijpers F. P., 2009, *A&A*, 494, 237
- Thévenin F., Kervella P., Pichon B., Morel P., di Folco E., Lebreton Y., 2005, *A&A*, 436, 253
- Thomas J. A., Hyland A. R., Robinson G., 1973, *MNRAS*, 165, 201
- Thompson G. I., Nandy K., Jamar C., Monfils A., Houziaux L., Carnochan D. J., Wilson R., 1978, *Catalogue of stellar ultraviolet fluxes. A compilation of absolute stellar fluxes measured by the Sky Survey Telescope (S2/68) aboard the ESRO satellite TD-1*
- Ulrich R. K., 1986, *ApJ*, 306, L37
- Valenti J. A., Fischer D. A., 2005, *ApJS*, 159, 141
- van Belle G. T., Ciardi D. R., Boden A. F., 2007, *ApJ*, 657, 1058
- van Belle G. T., von Braun K., 2009, *ApJ*, 694, 1085
- van Leeuwen F., 2007, *A&A*, 474, 653
- VandenBerg D. A., Clem J. L., 2003, *AJ*, 126, 778
- Vauclair S., Laymand M., Bouchy F., Vauclair G., Bon Hoa A. H., Charpinet S., Bazot M., 2008, *A&A*, 482, L5

APPENDIX A: COMPARISON WITH OTHER SPECTROSCOPIC STUDIES

In Tables A1–A3 we compare the atmospheric parameters from spectroscopic analysis (VWA) and Strömgren calibrations with values from the literature. Since we compare directly with similar spectroscopic techniques, we have not applied the -40 K offset to the T_{eff} from VWA (see Sect. 4.4). Each column is identified by the first author, i.e. Fuhrmann (1998, 2004, 2008), Sousa et al. (2008), Soubiran et al. (1998), Santos et al. (2004, 2005), and Valenti & Fischer (2005). We also list T_{eff} and $[\text{Fe}/\text{H}]$ using the Strömgren calibration by Holmberg et al. (2007).

APPENDIX B: PROJECTED ROTATIONAL VELOCITIES

In Table B1 we list $v \sin i$ and macroturbulence determined by the technique described in Sect. 5.5. Our results are in general agreement with similar investigations in the literature, identified by the first author in the Table: Saar & Osten (1997), Valenti & Fischer (2005), Reiners & Schmitt (2003), Dravins et al. (1993), and Allende Prieto et al. (2002). Only Saar & Osten (1997) determined both $v \sin i$ and macroturbulence with an approach similar to ours. Dravins et al. (1993) and Allende Prieto et al. (2002) used very high resolution spectra ($R \simeq 200\,000$) and compared their observed line profiles with 3D hydrodynamical simulations. It is encouraging that our method also matches the two later studies for β Hyi and Procyon A very well.

This paper has been typeset from a $\text{T}_{\text{E}}\text{X}/\text{L}^{\text{A}}\text{T}_{\text{E}}\text{X}$ file prepared by the author.

Table A1. Comparison of effective temperatures from this study (Strömgren, VWA) with values found in the literature as identified by the first author name.

Star	Strömgren	VWA	Fuhrmann	Sousa	Soubiran	Santos	Valenti
β Hyi	5870 \pm 70	5830 \pm 80					5873 \pm 44
τ Cet	5410 \pm 70	5330 \pm 80	5373 \pm 80	5310 \pm 17	5264 \pm 100	5344 \pm 29	5283 \pm 44
ι Hor	6110 \pm 70	6120 \pm 80				6252 \pm 53	6097 \pm 44
α For	6105 \pm 60	6055 \pm 80				6275 \pm 57	
δ Eri		5055 \pm 80	5044 \pm 80	5150 \pm 51		5074 \pm 60	
α Men	5580 \pm 70	5610 \pm 80				5594 \pm 36	5587 \pm 44
Procyon A	6595 \pm 70	6525 \pm 80	6470 \pm 80				
β Vir	6150 \pm 70	6090 \pm 80	6085 \pm 80		6109 \pm 75		
η Boo	6025 \pm 60	6070 \pm 80	6023 \pm 70				
γ Ser	6245 \pm 70	6155 \pm 80	6254 \pm 80				
μ Ara	5690 \pm 70	5705 \pm 80		5780 \pm 25		5798 \pm 33	
70 Oph A		5340 \pm 80	5310 \pm 80		5158 \pm 250		
η Ser		4890 \pm 80	4921 \pm 80		4859 \pm 250		
β Aql		5070 \pm 80	5110 \pm 90		5041 \pm 200		
δ Pav	5540 \pm 70	5590 \pm 80		5604 \pm 38			

Table A2. Comparison of the surface gravity from VWA with values found in the literature as identified by the first author name.

Star	VWA	Fuhrmann	Sousa	Soubiran	Santos	Valenti
β Hyi	3.84 \pm 0.08					4.08 \pm 0.06
τ Cet	4.46 \pm 0.08	4.54 \pm 0.10	4.44 \pm 0.03	4.36 \pm 0.30	4.57 \pm 0.09	4.59 \pm 0.06
ι Hor	4.40 \pm 0.08				4.61 \pm 0.16	4.34 \pm 0.06
α For	3.80 \pm 0.08				4.40 \pm 0.37	
δ Eri	3.77 \pm 0.08	3.84 \pm 0.10	3.89 \pm 0.08		3.77 \pm 0.16	
α Men	4.43 \pm 0.08				4.41 \pm 0.09	4.50 \pm 0.06
Procyon A	3.89 \pm 0.08	4.01 \pm 0.10				
β Vir	3.98 \pm 0.08	4.04 \pm 0.10		4.20 \pm 0.30		
η Boo	3.90 \pm 0.08	3.76 \pm 0.10				
γ Ser	4.01 \pm 0.08	4.02 \pm 0.10				
μ Ara	4.14 \pm 0.08		4.27 \pm 0.04		4.31 \pm 0.08	
70 Oph A	4.57 \pm 0.08	4.57 \pm 0.10		4.67 \pm 0.30		
η Ser	2.96 \pm 0.08	2.99 \pm 0.10		3.13 \pm 0.30		
β Aql	3.55 \pm 0.08	3.60 \pm 0.10		3.04 \pm 0.30		
δ Pav	4.32 \pm 0.08		4.26 \pm 0.06			

Table A3. Comparison of the metallicity from VWA with values found in the literature as identified by the first author name.

Star	Strömgren	VWA	Fuhrmann	Sousa	Soubiran	Santos	Valenti
β Hyi	-0.04 \pm 0.10	-0.10 \pm 0.07					-0.09 \pm 0.03
τ Cet	-0.42 \pm 0.10	-0.48 \pm 0.07	-0.53 \pm 0.07	-0.52 \pm 0.01	-0.50 \pm 0.15	-0.52 \pm 0.04	-0.36 \pm 0.03
ι Hor	-0.00 \pm 0.10	+0.15 \pm 0.07				+0.26 \pm 0.06	+0.09 \pm 0.03
α For	-0.16 \pm 0.10	-0.28 \pm 0.07				-0.19 \pm 0.06	
δ Eri		+0.15 \pm 0.07	+0.12 \pm 0.07	+0.13 \pm 0.04		+0.13 \pm 0.08	
α Men	+0.07 \pm 0.10	+0.15 \pm 0.07				+0.10 \pm 0.05	+0.05 \pm 0.03
Procyon A	+0.02 \pm 0.10	+0.01 \pm 0.07	-0.01 \pm 0.07				
β Vir	+0.10 \pm 0.10	+0.12 \pm 0.07	+0.14 \pm 0.09		+0.17 \pm 0.15		
η Boo	+0.27 \pm 0.10	+0.24 \pm 0.07	+0.28 \pm 0.07				
γ Ser	-0.19 \pm 0.10	-0.26 \pm 0.07	-0.19 \pm 0.07				
μ Ara	+0.19 \pm 0.10	+0.32 \pm 0.07		+0.30 \pm 0.02		+0.32 \pm 0.04	
70 Oph A		+0.12 \pm 0.07	+0.06 \pm 0.07		+0.03 \pm 0.15		
η Ser		-0.11 \pm 0.07	-0.21 \pm 0.07		-0.19 \pm 0.15		
β Aql		-0.21 \pm 0.07	-0.17 \pm 0.07		-0.04 \pm 0.15		
δ Pav	+0.33 \pm 0.10	+0.38 \pm 0.07		+0.33 \pm 0.03			

Table B1. The determined projected rotational velocity and macroturbulence from this study is compared with five other studies from the literature identified by the first author name. The unit is km s^{-1} for all measured parameters.

Star	This study $v \sin i$	This study v_{macro}	Saar $v \sin i$	Saar v_{macro}	Valenti $v \sin i$	Reiners $v \sin i$	Dravins $v \sin i$	Allende $v \sin i$
Sun	1.3 ± 0.6	2.4 ± 0.6	2.3 ± 0.6	1.9 ± 0.8				
β Hyi	2.7 ± 0.6	2.9 ± 0.6			4.0	3.3 ± 0.3	2 ± 1	
τ Cet	0.7 ± 0.6	0.9 ± 0.6	2.1 ± 0.4	0.4 ± 0.4	1.3	$< 1.8 \pm 0.1$		
ι Hor	5.3 ± 0.6	3.3 ± 0.6			6.5	4.2 ± 0.6		
α For	3.9 ± 0.6	3.7 ± 0.6				4.0 ± 0.7		
δ Eri	0.7 ± 0.6	0.9 ± 0.6				$< 2.3 \pm 0.5$		
α Men	0.6 ± 0.6	1.0 ± 0.6						
Procyon A	2.8 ± 0.6	4.6 ± 0.6			5.7			2.7
171 Pup	1.6 ± 0.6	1.9 ± 0.6						
ξ Hya	2.4 ± 0.6	3.8 ± 0.6						
β Vir	2.0 ± 0.6	3.6 ± 0.6						
η Boo	11.9 ± 0.6	5.3 ± 0.6				13.5 ± 1.3		
α Cen A	1.9 ± 0.6	2.3 ± 0.6	2.6 ± 0.9	2.7 ± 0.7	2.3			
α Cen B	1.0 ± 0.6	0.8 ± 0.6	1.0 ± 0.8	1.1 ± 0.8	0.9			
HR 5803	5.2 ± 0.6	4.1 ± 0.6				5.0 ± 0.2		
γ Ser	10.2 ± 0.6	3.9 ± 0.6				10.0 ± 1.3		
μ Ara	1.4 ± 0.6	2.6 ± 0.6				3.8 ± 0.2		
70 Oph A	0.9 ± 0.6	1.5 ± 0.6						
η Ser	1.1 ± 0.6	2.1 ± 0.6						
β Aql	0.9 ± 0.6	2.1 ± 0.6				$< 2.3 \pm 0.3$		
δ Pav	1.0 ± 0.6	1.7 ± 0.6				3.2 ± 0.2		
γ Pav	1.8 ± 0.6	2.0 ± 0.6				2.4 ± 0.5		
τ PsA	13.6 ± 0.6	4.1 ± 0.6				13.6 ± 0.2		
ν Ind	1.1 ± 0.6	1.4 ± 0.6						